Global Optimization Study of metal oxide nanoclusters and Their Application in Catalysis

Prof. Ramesh Ch. Deka

Department of Chemical Sciences

Tezpur University, Assam, India.


INDIA
States and Union Territories
N
TAJIKISTAN
AFGHANISTAN
PAKISTAN
CHINA
TIBET
NEPAL
BHUTAN
BANGLADESH
MYANMAR
SRI LANKA
Srinagar
JAMMU & KASHMIR
HIMACHAL PRADESH
Shimla
Chandigarh
PUNJAB
HARYANA
Dehradun
UTTARAKHAND
DELHI
Jaipur
RAJASTHAN
UTTAR PRADESH
Lucknow
Patna
BIHAR
SIKKIM
Gangtok
Itanagar
ARUNACHAL PRADESH
Dispur
Shillong
MEGHALAYA
ASSAM (Asom)
NAGALAND
Kohima
Imphal
MANIPUR
Agartala
TRIPURA
Aizawl
MIZORAM
Gandhinagar
GUJARAT
Bhopal
MADHYA PRADESH
JHARKHAND
Ranchi
WEST BENGAL
Kolkata
Raipur
CHHATTISGARH
ORISSA
Bhubaneshwar
Diu
Daman
Silvassa
DADRA & NAGAR HAVELI
Mumbai
MAHARASHTRA
BAY OF BENGAL
ARABIAN SEA
Hyderabad
ANDHRA PRADESH
Yanam (Puducherry)
Panaji
GOA
KARNATAKA
Bengaluru
Chennai
Puducherry
Mahe (Puducherry)
Kavaratti
LAKSHADWEEP (INDIA)
KERALA
TAMIL NADU
Karaikal (Puducherry)
Thiruvananthapuram
ANDAMAN & NICOBAR ISLANDS (INDIA)
Port Blair
LEGEND
International Boundary
State Boundary
National Capital
State & U.T. Capital
Map not to Scale
Copyright © 2007 Compare Infobase Limited
INDIAN OCEAN

Kaziranga

Outline

- **Metal and metal oxide clusters, their importances**
- **Global optimization methods using atomistic and DFT methods**
- Metal clusters in catalysis:
  - **CO oxidation**
  - **NO oxidation**
  - **Methane oxidation**
- **Hydrogen spillover using ONIOM method in zeolites**
- **Encapsulation of transition metal complexes of Fe, Co, Ni, Cu, and Zn inside zeolite- Y.**
- **Assessing the catalytic behaviour of the neat and encapsulated complexes and to study the reaction mechanism using DFT calculation.**
- **Conclusion**

Activities of the Group

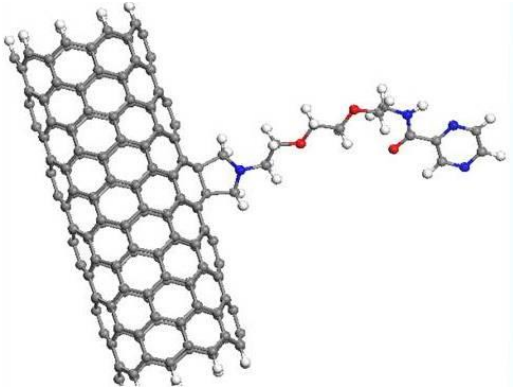

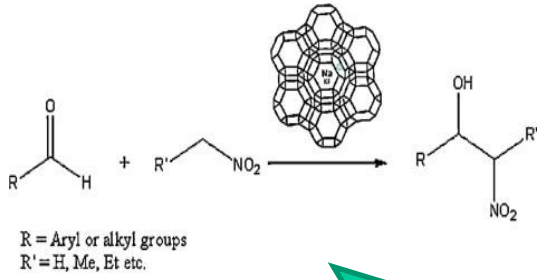

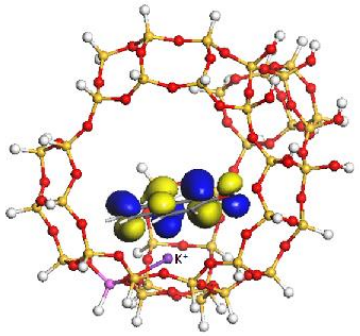

Synthesis &
Application of Zeolite Catalysis

Nanotube, Drug Design
& Delivery

Modeling Zeolite Supported
Metal Catalysis

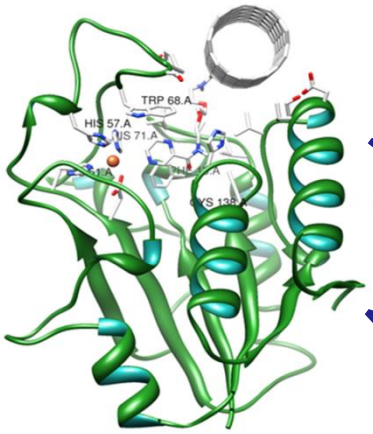

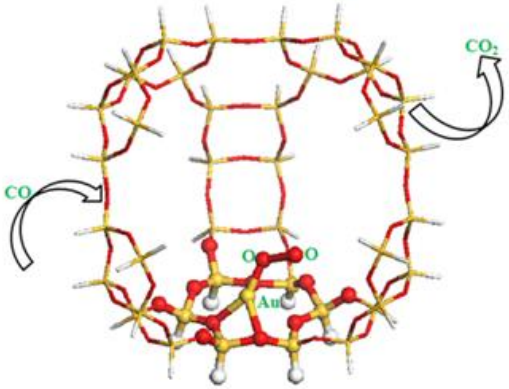

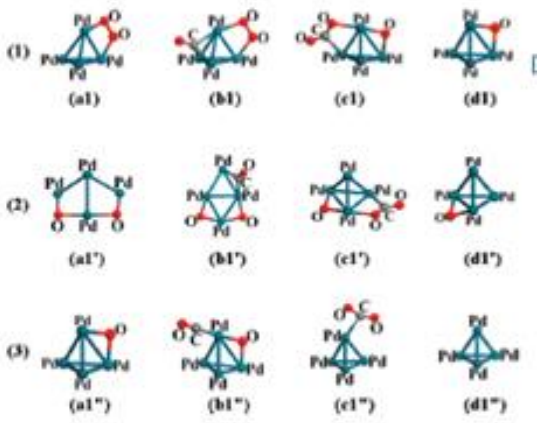

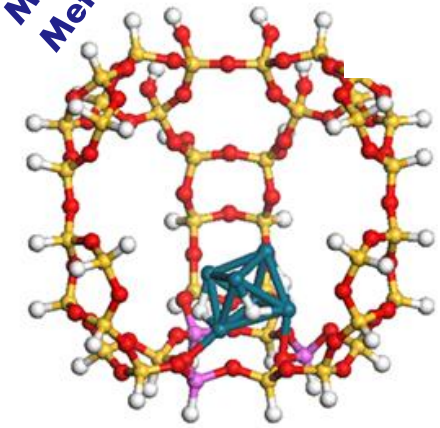

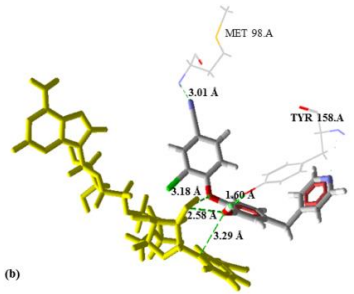

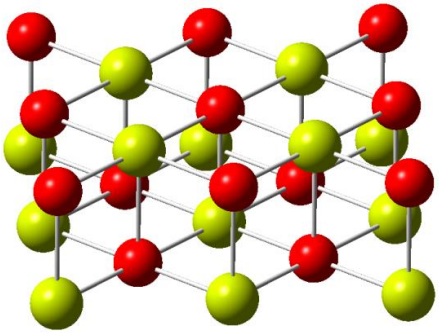

Modeling
Metal Oxides

Metal and Metal Oxide Nanoclusters

Nanoclusters of metals and metal oxides are used as:

- Catalysis
  - Exhibit versatile acid-base and redox properties
  - Catalyze many reactions: dehydration, partial/selective reduction or oxidation, photo- or electro-chemical reactions, etc.
  - Supported catalysts for enhanced reactivity, selectivity, and catalyst utilization
- Solar cells
- Magnetic Nanoclusters
  - recording media
  - components of miniature electronic devices
  - sensors
  - ferrofluids
- Labeling agents and carriers in biology
- Diagnostic and therapeutic tools in medicine.

Cluster Size Regimes

MACROSCOPIC — MESOSCOPIC — MICROSCOPIC

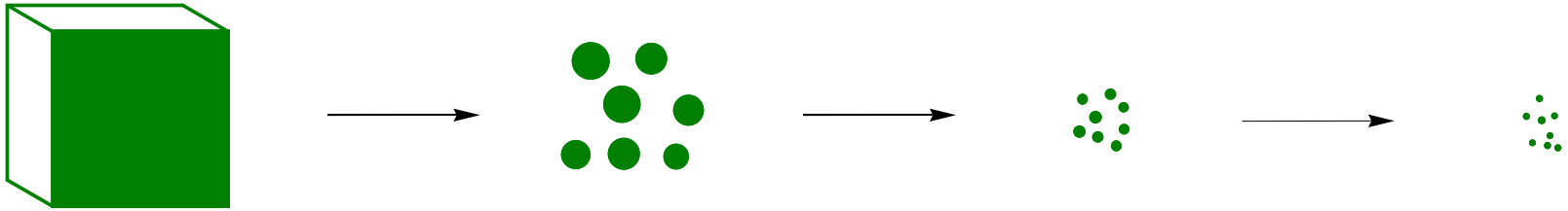

$D > 10^4$ Å

$N > 10^{10}$

BULK

$D \sim 10^2\text{-}10^4$ Å

$N \sim 10^4\text{-}10^{10}$

COLLOIDS

$D \sim 10\text{-}10^2$ Å

$N \sim 10\text{-}10^4$

NANOCLUSTERS

$D < 10$ Å

$N < 10$

ATOMS & MOLECULES

Reduction of 4-Nitrophenol to 4-Aminophenol over metallic nanoclusters

Importance of 4-aminophenol

- **a photographic developer**
- **corrosion inhibitor**
- **an important intermediate for the manufacture of analgesic and antipyretic drugs**
- **anticorrosion-lubricant**
- **hair-dyeing agent**

P Deka, RC Deka and P Bharali, *New J. Chem.*, **2014**, 38 (4), 1789-1793.

NJC Editorial, 21 December, 2015
Highlights of 2015

Table 2 Papers published in *NJC* in 2014 that received at least 11 citations in 2015[a]

DOI	Title	Authors
10.1039/c4nj00864b	Bioinspired nanoarchitectonics as emerging drug delivery systems	Katsuhiko Ariga, Kohsaku Kawakami, Mitsuhiro Ebara, Yohei Kotsuchibashi, Qingmin Ji, Jonathan P. Hill
10.1039/c4nj01440e	Green synthesis and catalytic properties of palladium nanoparticles for the direct reductive amination of aldehydes and hydrogenation of unsaturated ketones	Mahmoud Nasrollahzadeh
10.1039/c3nj01558k	Enhanced activity of a hydrothermally synthesized mesoporous MoS_2 nanostructure for high performance supercapacitor applications	Ananthakumar Ramadoss, Taehyun Kim, Gui-Shik Kim, Sang Jae Kim
10.1039/c4nj00816b	Facilely constructing 3D porous $NiCo_2S_4$ nanonetworks for high-performance supercapacitors	Yang Liu, Jianan Zhang, Shoupei Wang, Kaixi Wang, Zhimin Chen, Qun Xu
10.1039/c3nj01556d	Water and methanol adsorption on MOFs for cycling heat transformation processes	Felix Jeremias, Dominik Fröhlich, Christoph Janiak, Stefan K. Henninger
10.1039/c3nj01368e	Nano-$CoFe_2O_4$ supported molybdenum as an efficient and magnetically recoverable catalyst for a one-pot, four-component synthesis of functionalized pyrroles	Bao-Le Li, Mo Zhang, Hai-Chuan Hu, Xia Du, Zhan-Hui Zhang
10.1039/c3nj01589k	*In situ* generated copper nanoparticle catalyzed reduction of 4-nitrophenol	Pangkita Deka, Ramesh C. Deka, Pankaj Bharali
10.1039/c3nj00667k	Triazolium cations: from the "click" pool to multipurpose applications	Jesus M. Aizpurua, Raluca M. Fratila, Zaira Monasterio, Nerea Pérez-Esnaola, Elena Andreieff, Aitziber Irastorza, Maialen Sagartzazu-Aizpurua
10.1039/c3nj00535f	Diamondoids: functionalization and subsequent applications of perfectly defined molecular cage hydrocarbons	Maria A. Gunawan, Jean-Cyrille Hierso, Didier Poinsot, Andrey A. Fokin, Natalie A. Fokina, Boryslav A. Tkachenko, Peter R. Schreiner

Oxidative Degradation of Organic dye Pollutants over porous Metal Oxide nanostructure

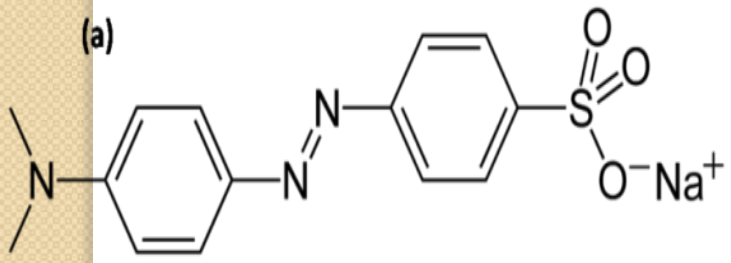

Methyl Orange (MO)

Exhibits the maximum absorption band centred at 465 nm.

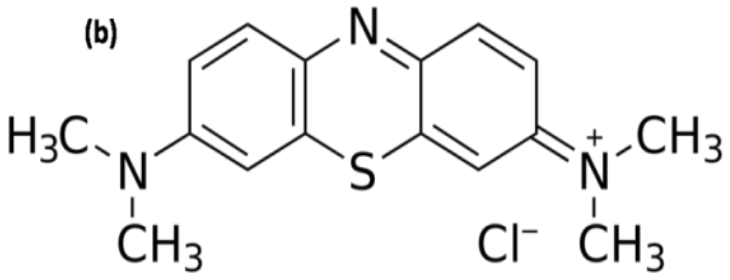

Methylene Blue (MB)

Exhibits the maximum absorption band centred at 664 nm.

P Deka, RC Deka and P Bharali, *New J. Chem.*, **2016**, 40 (1), 348-357.

Importance of Theory

- Many cluster properties (e.g. cluster geometries, binding energies and energy barriers) are not easily measured directly from experiment.

- Chemical and physical properties of nanoclusters are substantially different from bulk phases

- Understanding possible structural changes as a function of the size of nanocluster can lead to the discovery of new materials with desirable properties

- Theoretical models ahd computational methods have been very useful in helping to interpret spectroscopic (e.g. UV/ visible and photoelctron) and mass spectrometric data

Computational Studies of Nanoclusters

- Computer simulations are often used as a complementary predictive tool or an aid in the analysis of experimental observations

Global Optimisation Techniques:

- Monte-Carlo basin hopping
- Random quenching
- Simulated annealing
- Evolutionary algorithms (genetic algorithms) and
- Particle swarm algorithms

Knowledge Led Master Code (KLMC) program

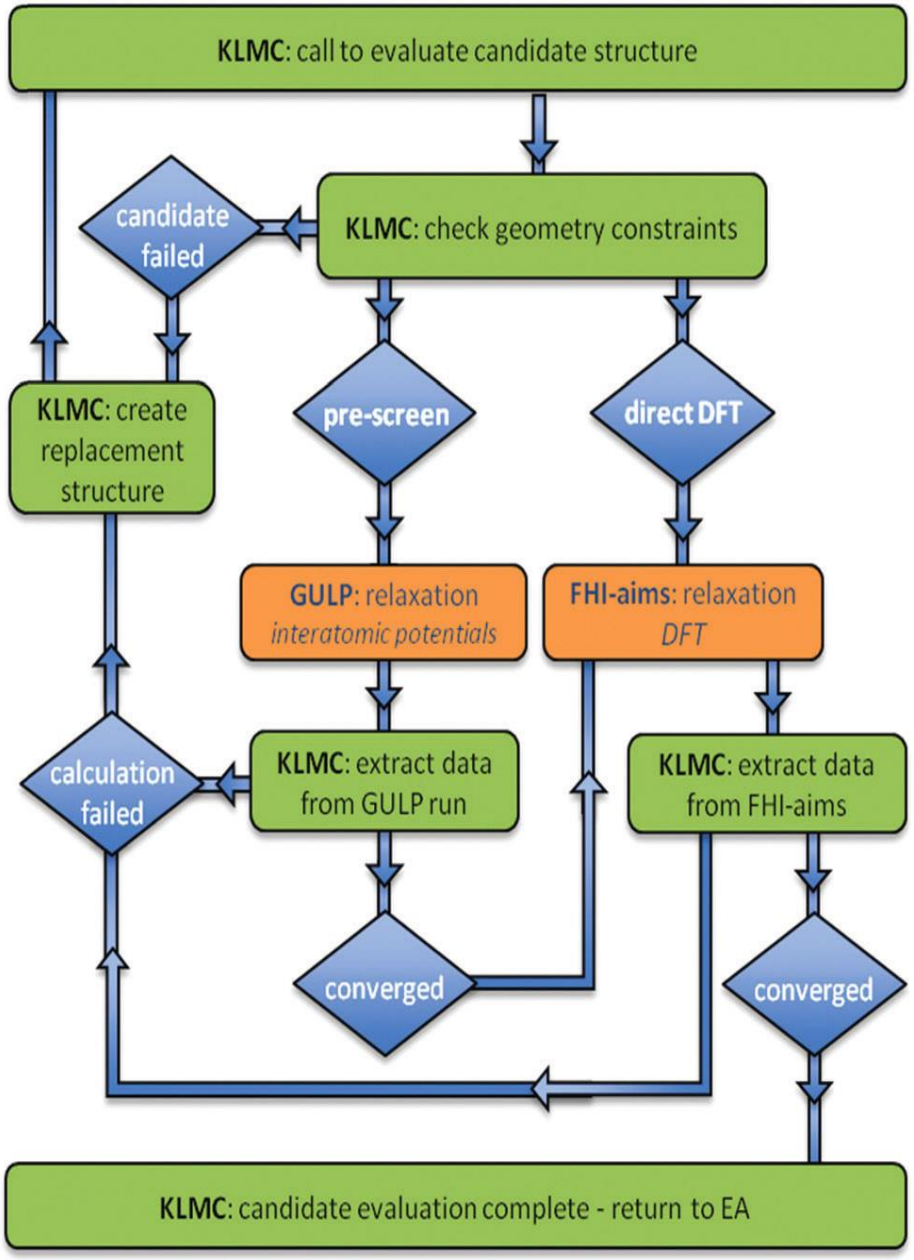

M. R. Farrow, Y. Chow and S. M. Woodley,
*Phys. Chem. Chem. Phys., 2014, **16**, 21119--21134*

Flow chart of the evaluation process as implemented by KLMC. Green represents actions solely undertaken by KLMC; orange – actions undertaken by third party software; and blue – user-defined choice or main result of an action.

Two to six atom clusters

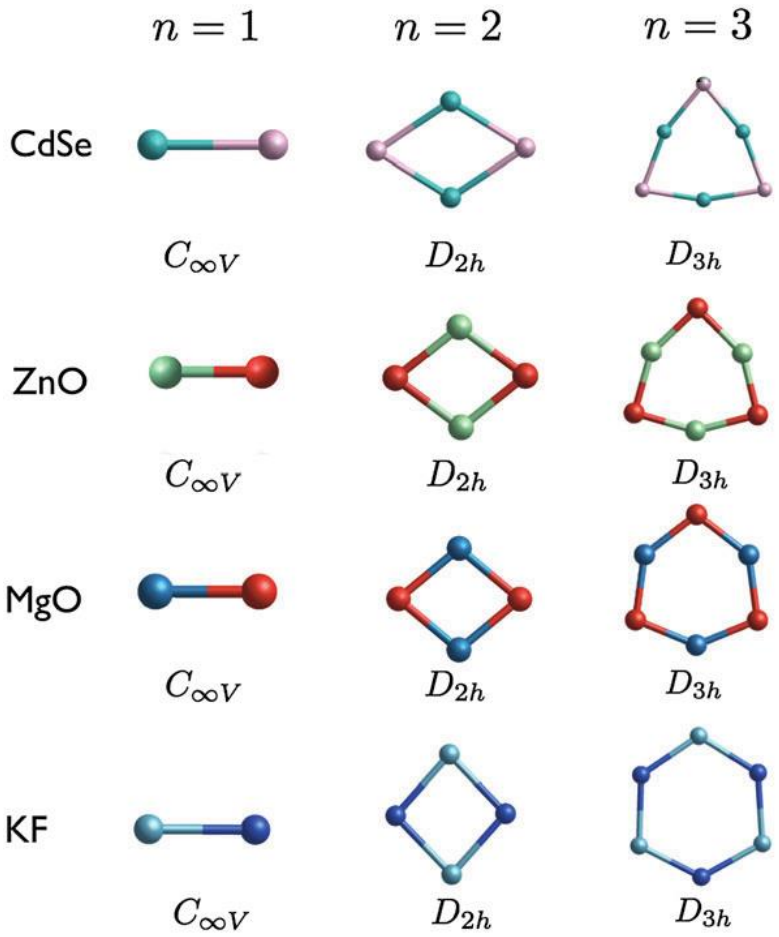

ZnO and MgO- catalysts

KF – brazing aluminiu

CdSe – solar cells

CdSe- strongly polarisable

KF – weakly polarisable

Shape of n=3 ring for KF compare to rigid ion model of ZnO

Diff. in electronegativity, ratio of inoic radii, bond dissociation energy and refractive index

Compound	$X_B - X_A$	R_B/R_A	D (kJ mol^{-1})	n_r
CdSe	0.86	2.08	123.9	65.67
ZnO	1.79	1.89	$\leq$246.3	75.40
MgO	2.13	1.94	354.5	80.04
KF	3.16	0.96	485.5	94.66

FHI-aims calculated structural parameters

Compound	L_1 (Å)	E_b (eV)	L_2 (Å)	θ (°)
CdSe	2.35	2.04	2.46	65.67
ZnO	1.68	3.80	1.87	75.40
MgO	1.73	4.39	1.90	80.04
KF	2.17	6.37	2.36	94.66

CdSe has the weakest bond, ZnO and MgO, the second and third, whereas KF has the strongest bond

Eight to ten atom clusters

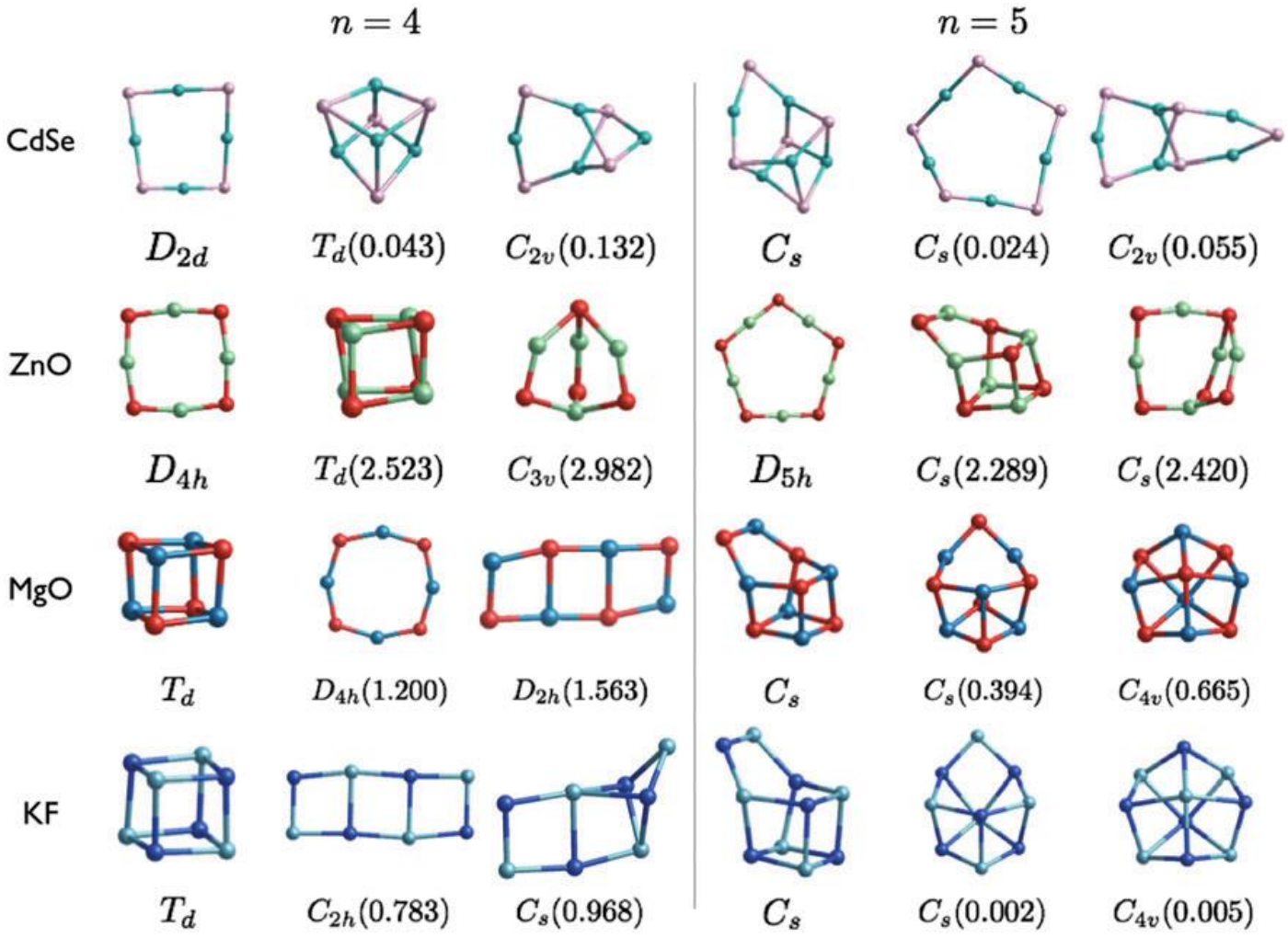

Same GM for CdSe, MgO and KF

2D to 3D occurs earlier for MgO and KF

GM: For n=4 ZnO and CdSe have ring, LM2- cuboid

GM: Cuboid for MgO and KF, From a KF cuboid to a CdSe ring

Twelve to fourteen atom clusters

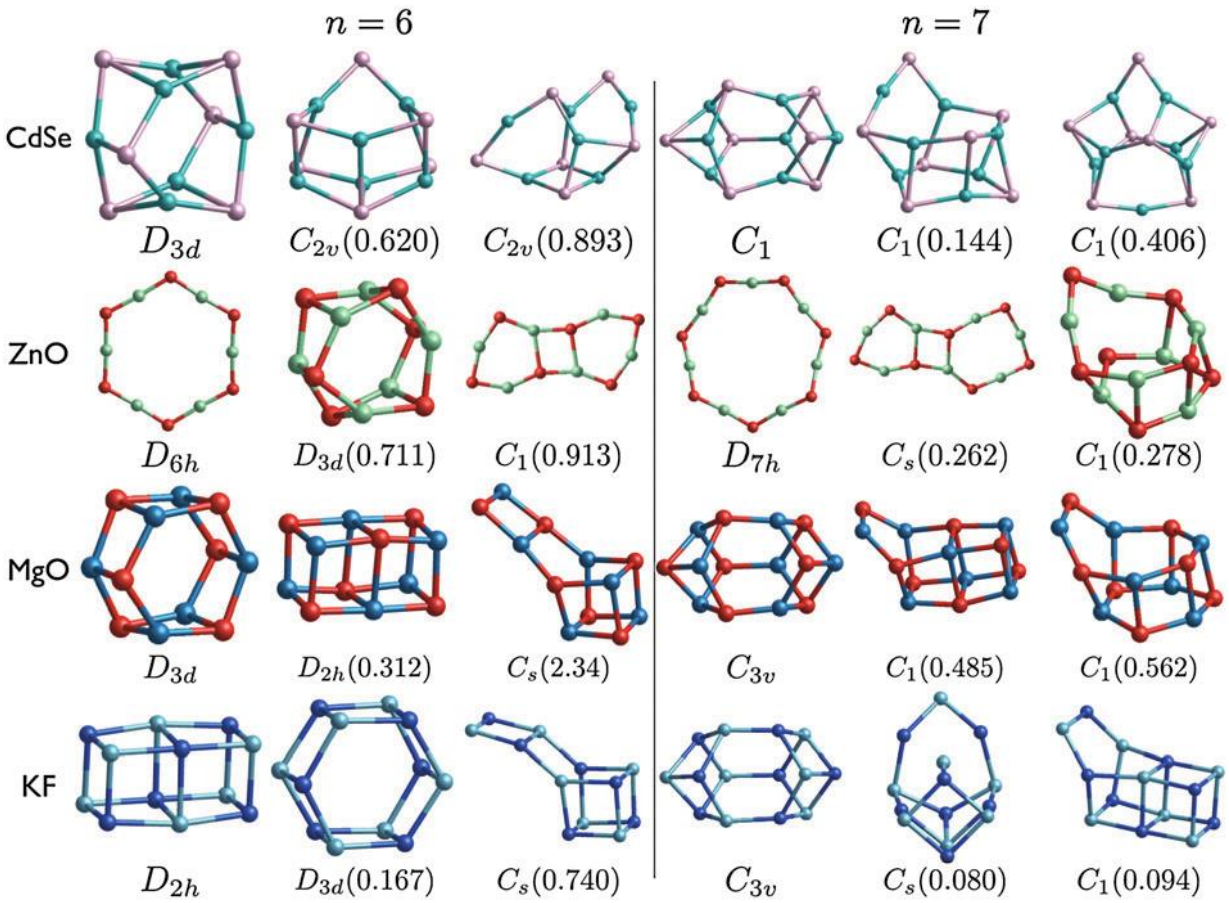

ZnO retains 2D ring as GM for n = 7

ZnO retains the 2D ring motif as GM. For n=6, MgO, drum (double ring), tube and rock-salt cut.

Sixteen to eighteen atom clusters

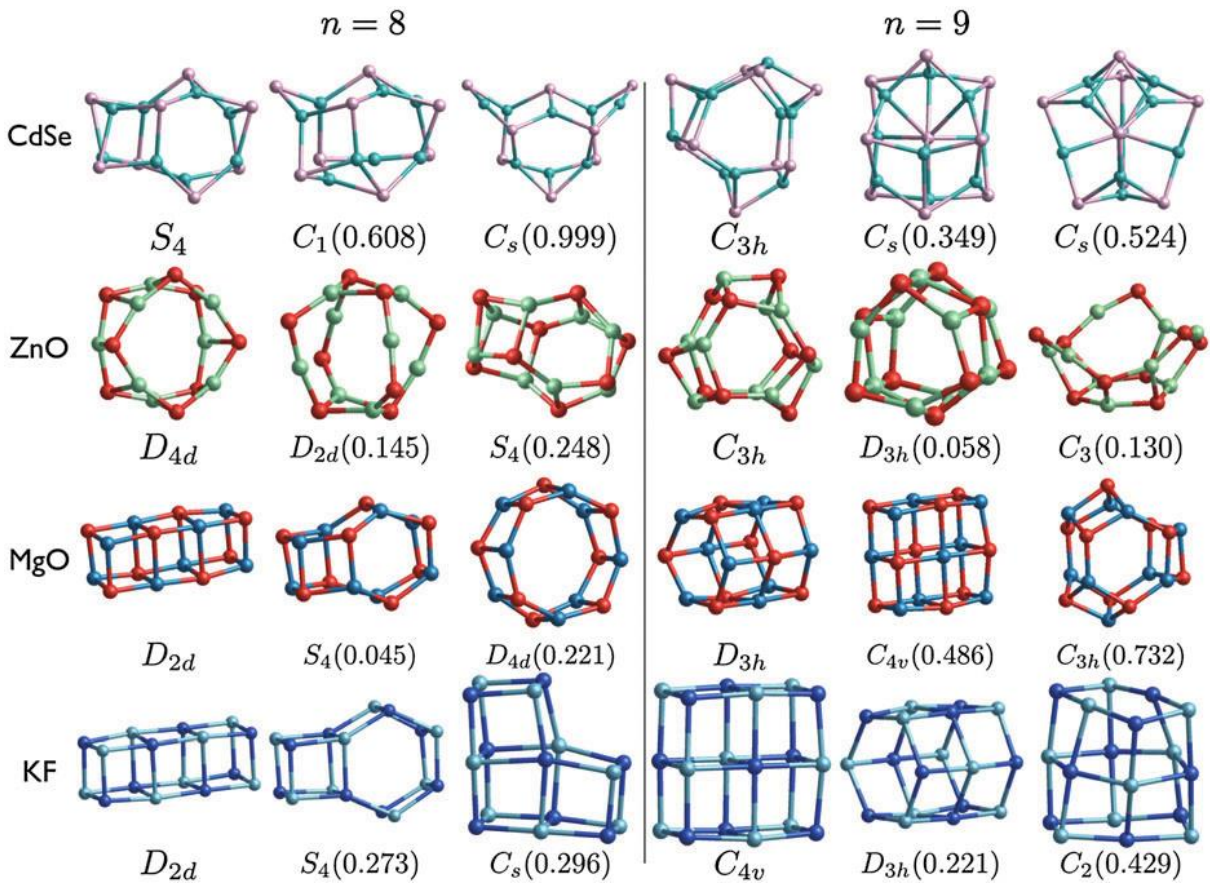

The transition of ZnO GM to a 3D occurs between n=7 and 8

Twenty to twenty two atom clusters

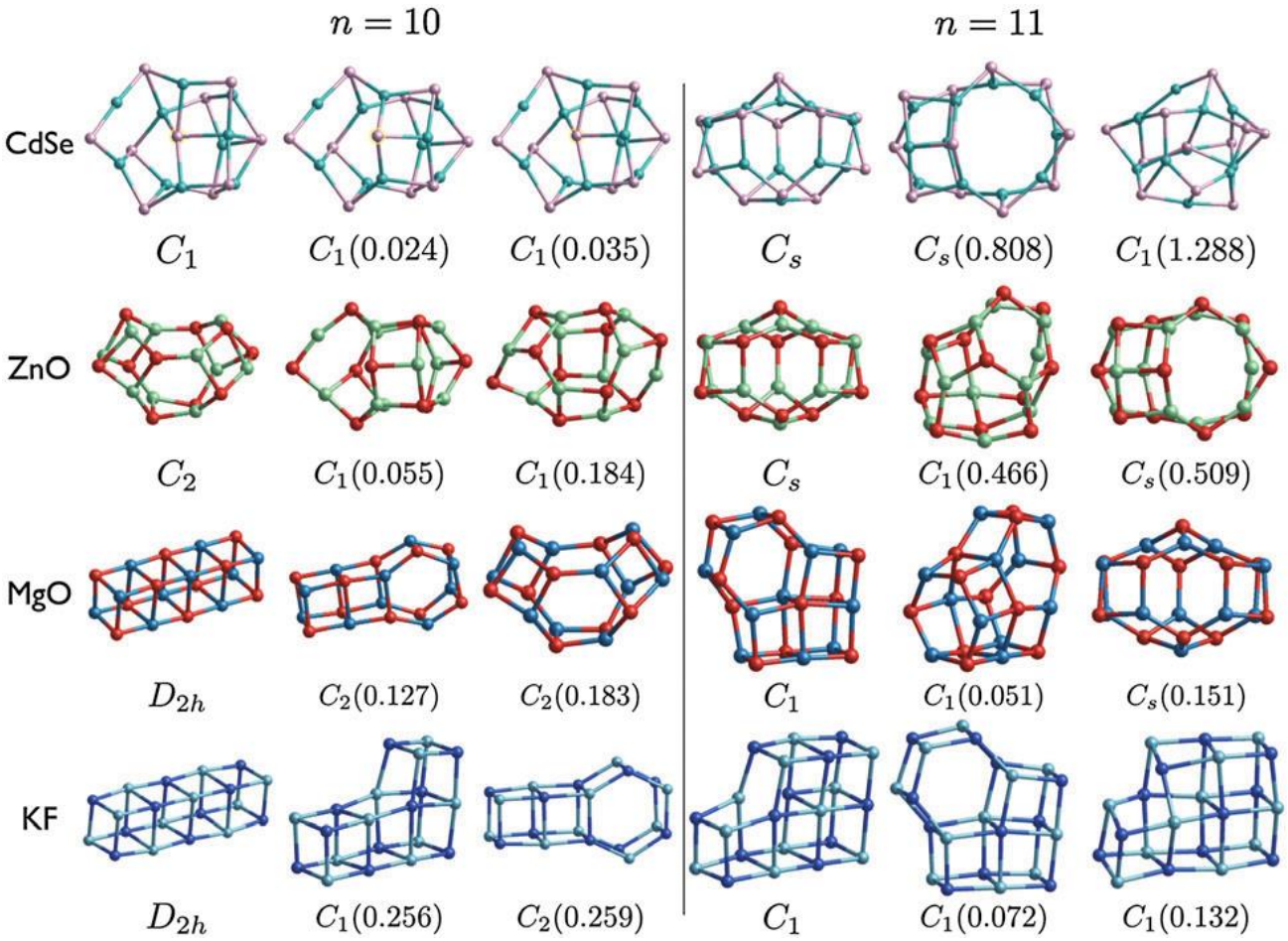

For n=10, MgO and KF have same motif for their GM, however, LM2 of MgO is LM3 of KF. The GM of $(MgO)_{11}$ is the LM2 of $(KF)_{11}$. Similarities between MgO KF continue.

Twenty four atom clusters

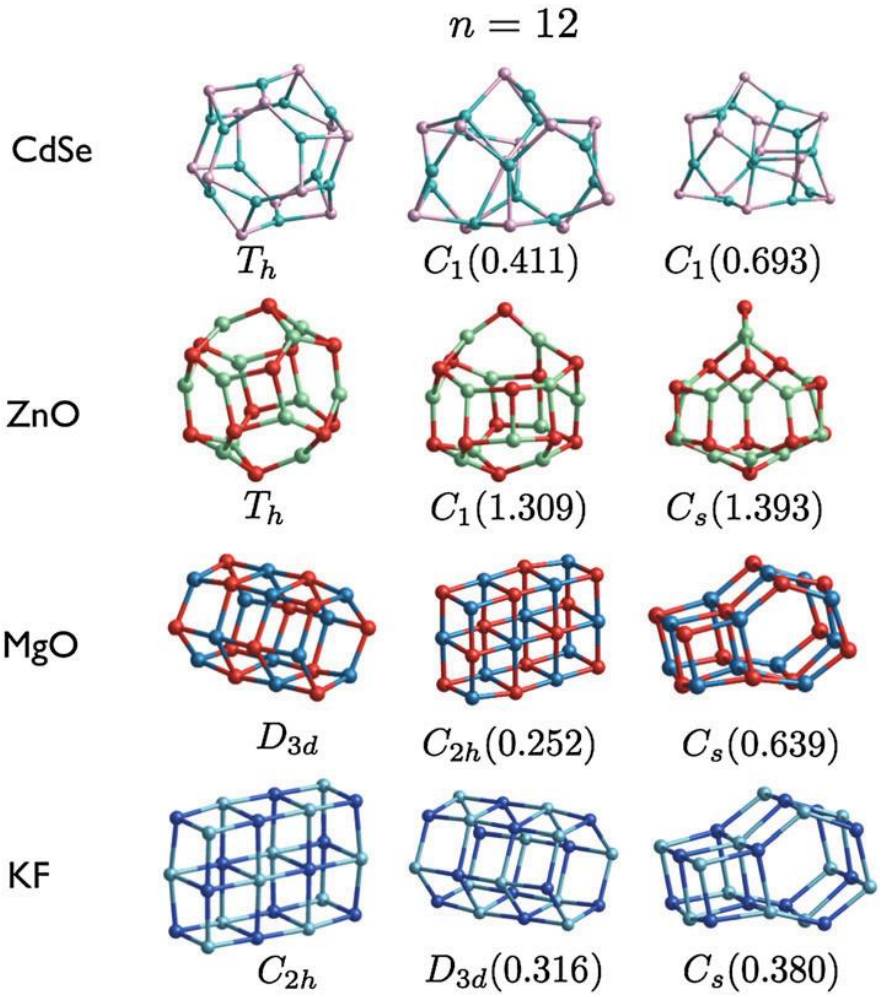

Similarities between MgO and KF continue for n=12, where apart from the change in ranking, the clusters have the same motifs. GM of $(MgO)_{12}$ is a tube.

Properties of Global Minima Clusters

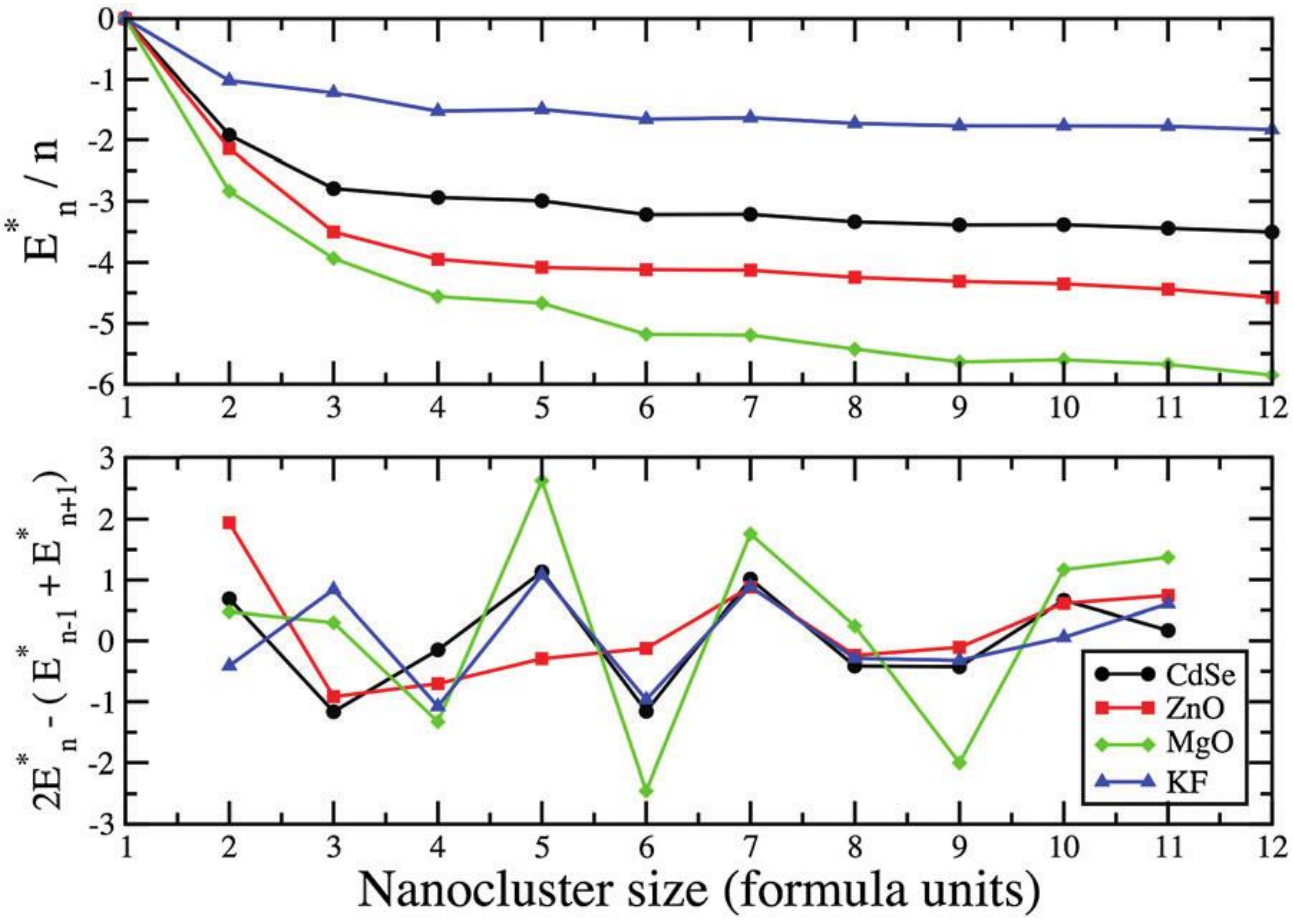

$E_n^* = E_n - nE_1$

Energy decreases with cluster size, reaching the bulk values, e.g. -7.64 eV per MgO
Second energy differences (SED) shows three minima, greater stability for (MgO)n at n=4 (cuboid), 6 (drum) and 9 (tube) which correlates to the reproduction of a larger quantity of these sizes when (MgO)n clusters are synthesized.

Average Bond Lengths and Coordination numbers

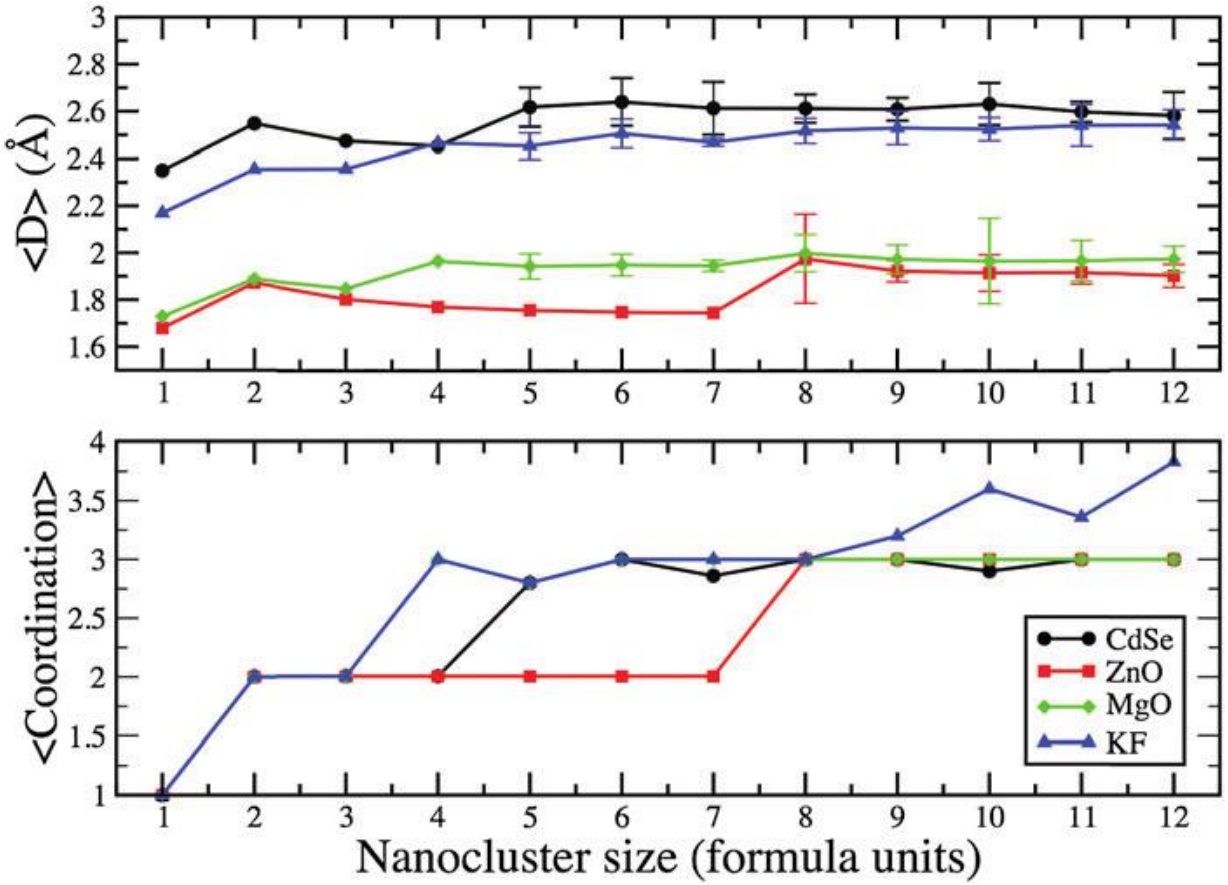

Average coordination number of the constituent atoms gradually increases for KF clusters, dimensionality of the cluster (1D, 2D then 3D, longer plateau for 2D $(ZnO)_n$.

The average bond distance, <D> also increases when the dimensionality of the cluster increases, but gradually decreases with increasing n

HOMO and LUMO energies for ZnO and MgO in eV

	ZnO			MgO		
n	E_{HOMO}	E_{LUMO}	ΔE	E_{HOMO}	E_{LUMO}	ΔE
2	−5.65	−4.35	1.30	−4.57	−3.13	1.45
3	−6.46	−3.03	3.03	−5.44	−2.61	2.83
4	−6.32	−3.25	3.06	−4.97	−2.51	2.45
5	−6.46	−3.35	3.12	−4.88	−2.79	2.10
6	−6.28	−3.06	3.06	−5.29	−2.28	3.01
7	−6.37	−3.28	3.28	−5.10	−2.48	2.61
8	−6.20	−3.63	2.57	−4.98	−2.30	2.68
9	−6.02	−3.88	2.15	−5.39	−2.20	3.18
10	−6.05	−2.21	2.21	−4.97	−2.25	2.72
11	−6.01	−2.11	2.11	−5.15	−2.33	2.81
12	−6.33	−2.52	2.52	−5.45	−2.17	3.28
Bulk	—	—	3.44[a]	—	—	7.77[b]

a) U. Ozgur et al, J. Appl. Phys, 2005, 98, 103 b) D.M. Roessler and W. C. Walker, Phys. Rev., 1967, 159, 733.

For ZnO, ΔE shows a transition between n=7 and 8, which directly correlates with the 2D to 3D structural transition. Similarly, the 2D-3D transitions occurs at n=3-4 for MgO and can be seen as a drop in ΔE. The smaller 3D structures of MgO are observed to have a smaller ΔE.

HOMO and LUMO energies for KF and CdSe in eV

	KF			CdSe		
n	E_{HOMO}	E_{LUMO}	ΔE	E_{HOMO}	E_{LUMO}	ΔE
2	−5.32	−0.35	4.97	−5.17	−3.92	1.26
3	−5.47	−0.25	5.22	−5.64	−3.09	2.55
4	−5.67	−0.12	5.55	−5.63	−3.02	2.61
5	−5.32	−0.44	4.89	−5.27	−3.64	1.63
6	−5.58	−0.17	5.41	−5.64	−3.47	2.17
7	−5.67	−0.28	5.40	−5.46	−3.43	2.03
8	−5.61	−0.17	5.44	−5.69	−3.42	2.27
9	−5.50	−0.23	5.28	−5.75	−3.43	2.31
10	−5.58	−0.31	5.27	−5.19	−3.38	1.81
11	−5.47	−0.41	5.06	−5.71	−3.45	2.26
12	−5.52	−0.21	5.31	−5.92	−3.40	2.52
~10 Å	—	—	—	—	—	3.00[a]
Bulk	—	—	10.9[b]	—	—	1.86[c]
						1.74[d]

a) J. Am. Chem. Soc. 1993, 115, 8706, b) J. Appl. Phys. 1966, 17, 1553, c) Nano Lett., 2001, 1 349, d) J. Am. Chem. Soc. 2000, 122, 2673

The calculated ΔE for KF is nearly constant around 5 eV which is about half the reported bulk value. N=5 includes lower coordinated ions, shows a drop in ΔE. Calculated ΔE for CdSe for the larger nanoclusters is comparable with the absorption edge experimentally observed for the smallest nanoparticles of about 3 eV.

Global Optimization of other Metal Oxides

- Global optimisation of different clusters of $(NiO)_n$, $(CeO_2)_n$ $(SnO_2)_n$ with KLMC code

- Calculations at the interatomic potential level of theory are performed by the General Utility Lattice Program (GULP), whereas for the DFT level FHI-aims and ORCA are employed.

Cerium Oxide Nanoclusters

$(CeO_2)_n$ global minimum (GM) nanoclusters, as determined on the PBEsol energy landscapes, for n = 1–20, arranged by size for the top 3 structures.

Colours: light green is Ce and red is O.

Energy differences from the GM (in eV) are given in brackets

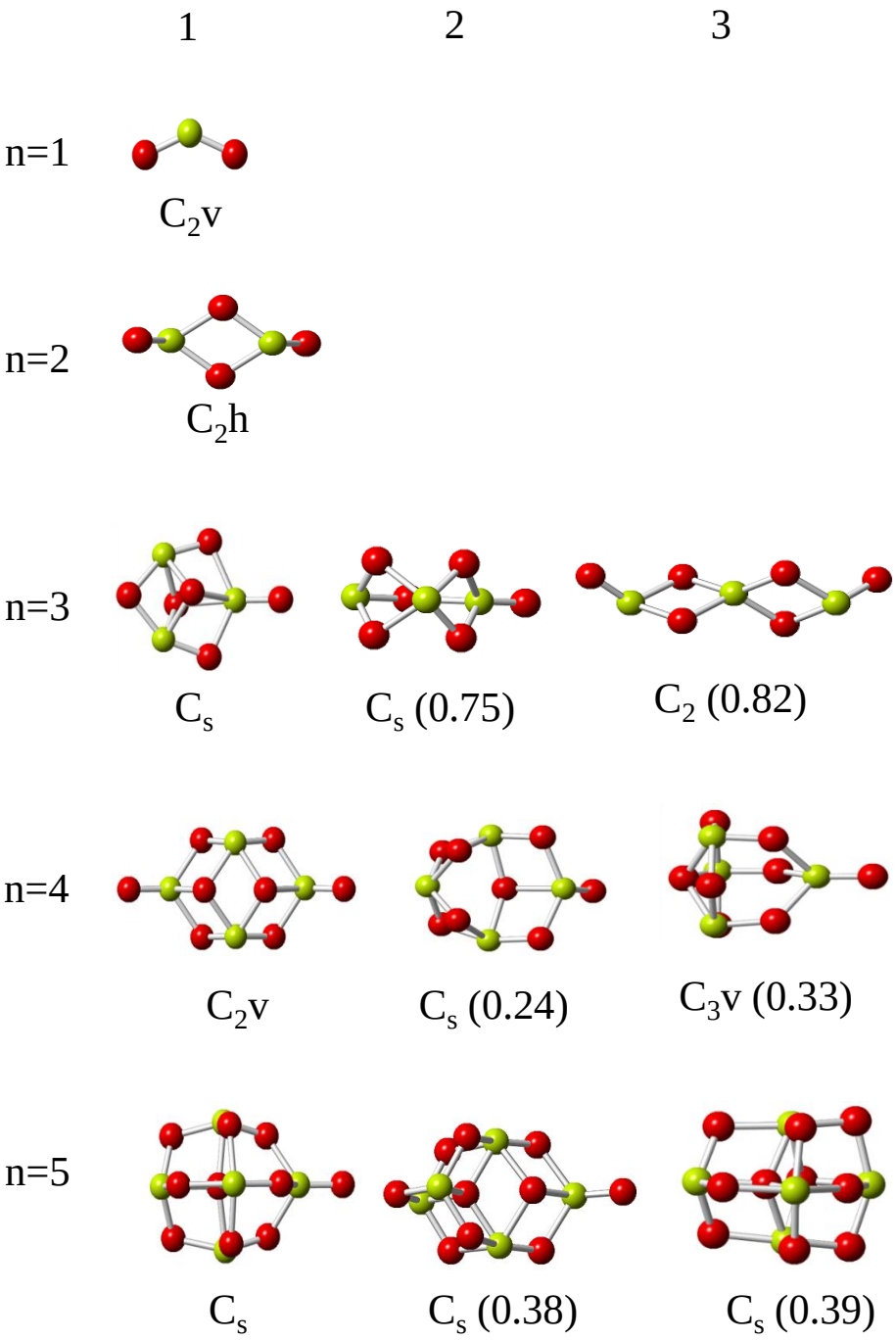
1
2
3
n=1
C2v
n=2
C2h
n=3
Cs
Cs (0.75)
C2 (0.82)
n=4
C2v
Cs (0.24)
C3v (0.33)
n=5
Cs
Cs (0.38)
Cs (0.39)

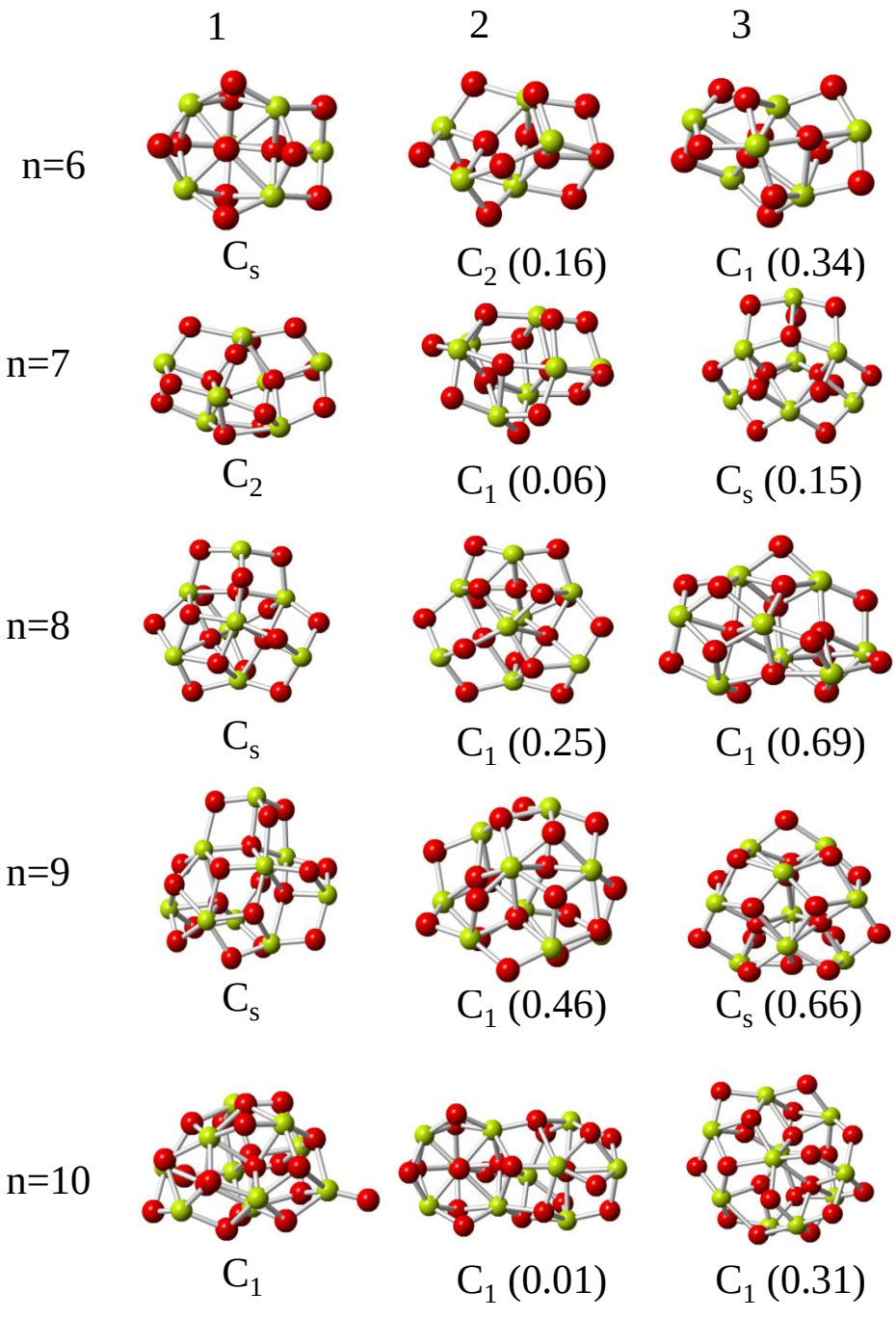
1
2
3
n=6
Cs
C2 (0.16)
C1 (0.34)
n=7
C2
C1 (0.06)
Cs (0.15)
n=8
Cs
C1 (0.25)
C1 (0.69)
n=9
Cs
C1 (0.46)
Cs (0.66)
n=10
C1
C1 (0.01)
C1 (0.31)

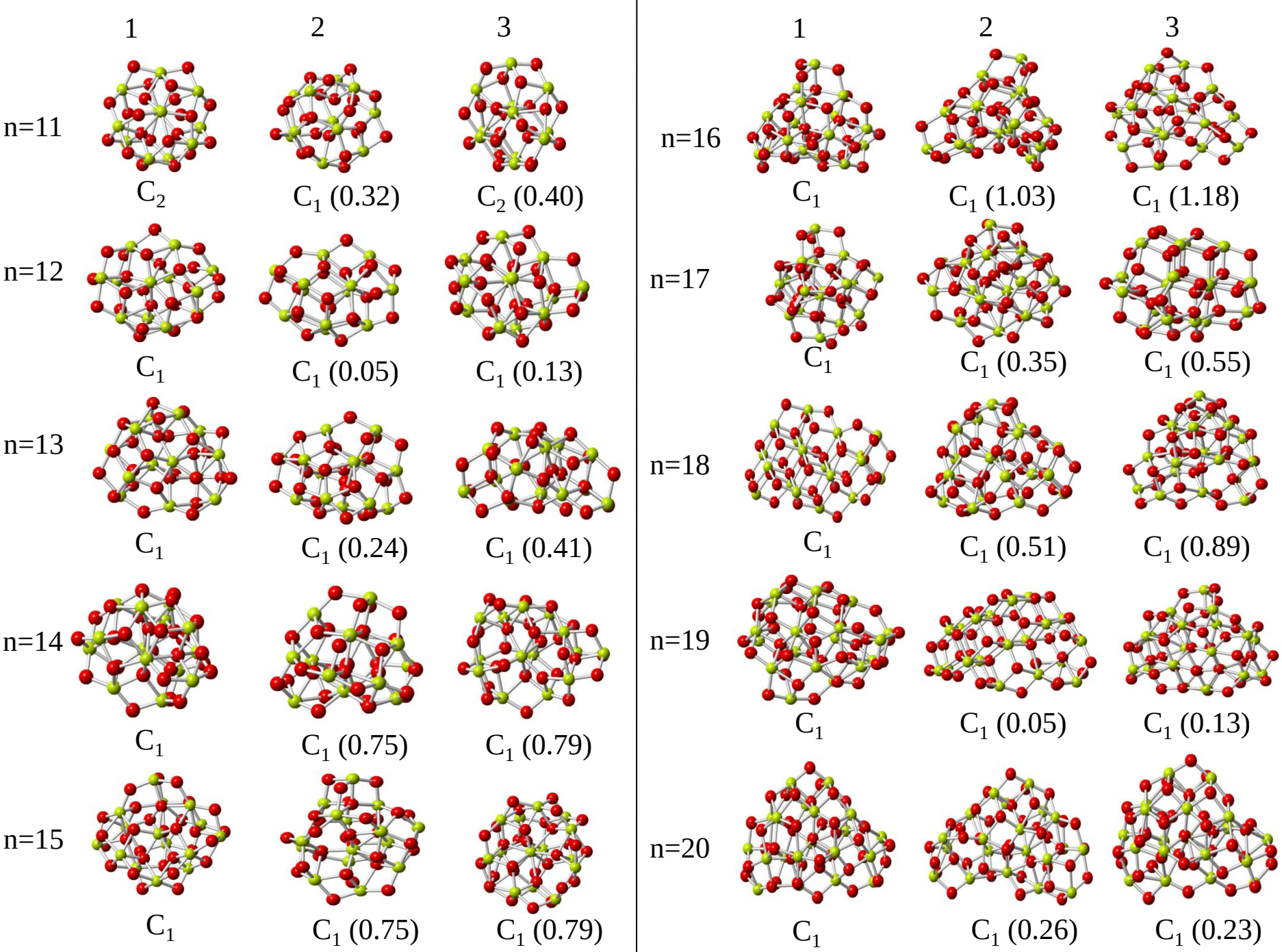
1
2
3
n=11
C2
C1 (0.32)
C2 (0.40)
n=12
C1
C1 (0.05)
C1 (0.13)
n=13
C1
C1 (0.24)
C1 (0.41)
n=14
C1
C1 (0.75)
C1 (0.79)
n=15
C1
C1 (0.75)
C1 (0.79)
1
2
3
n=16
C1
C1 (1.03)
C1 (1.18)
n=17
C1
C1 (0.35)
C1 (0.55)
n=18
C1
C1 (0.51)
C1 (0.89)
n=19
C1
C1 (0.05)
C1 (0.13)
n=20
C1
C1 (0.26)
C1 (0.23)

Table. Energy (eV) of the top three structures from FHI-aims calculation

	1st	2nd	3rd
CeO_2	-249513.23		
Ce_2O_4	-499029.20		
Ce_3O_6	-748545.81	-748545.06	-748544.99
Ce_4O_8	-998062.10	-998061.88	-998061.77
Ce_5O_{10}	-1247579.58	-1247579.21	-1247579.19
Ce_6O_{12}	-1497096.75	-1497096.58	-1497096.41
Ce_7O_{14}	-1746613.90	-1746613.85	-1746613.76
Ce_8O_{16}	-1996131.18	-1996130.93	-1996130.49
Ce_9O_{18}	-2245647.66	-2245647.20	-2245647.00
$Ce_{10}O_{20}$	-2495164.80	-2495164.79	-2495164.49
$Ce_{11}O_{22}$	-2744682.33	-2744682.00	-2744681.93
$Ce_{12}O_{24}$	-2994199.37	-2994199.32	-2994199.24
$Ce_{13}O_{26}$	-3243716.21	-3243715.96	-3243715.80
$Ce_{14}O_{28}$	-3493233.87	-3493233.12	-3493233.07
$Ce_{15}O_{30}$	-3742750.76	-3742750.34	-3742750.23
$Ce_{16}O_{32}$	-3992268.00	-3992266.98	-3992266.83
$Ce_{17}O_{34}$	-4241784.46	-4241784.11	-4241783.91
$Ce_{18}O_{36}$	-4491302.27	-4491301.76	-4491301.38
$Ce_{19}O_{38}$	-4740818.90	-4740818.85	-4740818.77
$Ce_{20}O_{40}$	-4990335.38	-4990335.12	-4990335.15

The energy of HOMO and LUMO, and their difference ΔE, CeO_2 for GM

	E_{HOMO} (eV)	E_{LUMO} (eV)	ΔE (eV)
CeO_2	-5.137	-2.928	2.209
Ce_2O_4	-5.885	-3.589	2.296
Ce_3O_6	-5.567	-3.698	1.869
Ce_4O_8	-5.833	-4.071	1.762
Ce_5O_{10}	-5.489	-3.844	1.645
Ce_6O_{12}	-5.503	-3.664	1.839
Ce_7O_{14}	-5.643	-3.566	2.077
Ce_8O_{16}	-5.723	-3.780	1.943
Ce_9O_{18}	-5.634	-3.800	1.834
$Ce_{10}O_{20}$	-5.389	-3.957	1.432
$Ce_{11}O_{22}$	-5.533	-3.711	1.822
$Ce_{12}O_{24}$	-5.507	-3.807	1.700
$Ce_{13}O_{26}$	-5.491	-3.896	1.595
$Ce_{14}O_{28}$	-5.587	-3.939	1.647
$Ce_{15}O_{30}$	-5.580	-3.867	1.713
$Ce_{16}O_{32}$	-5.767	-4.050	1.718
$Ce_{17}O_{34}$	-5.328	-3.837	1.491
$Ce_{18}O_{36}$	-5.391	-4.007	1.383
$Ce_{19}O_{38}$	-5.578	-3.843	1.735
$Ce_{20}O_{40}$	-5.458	-3.919	1.538

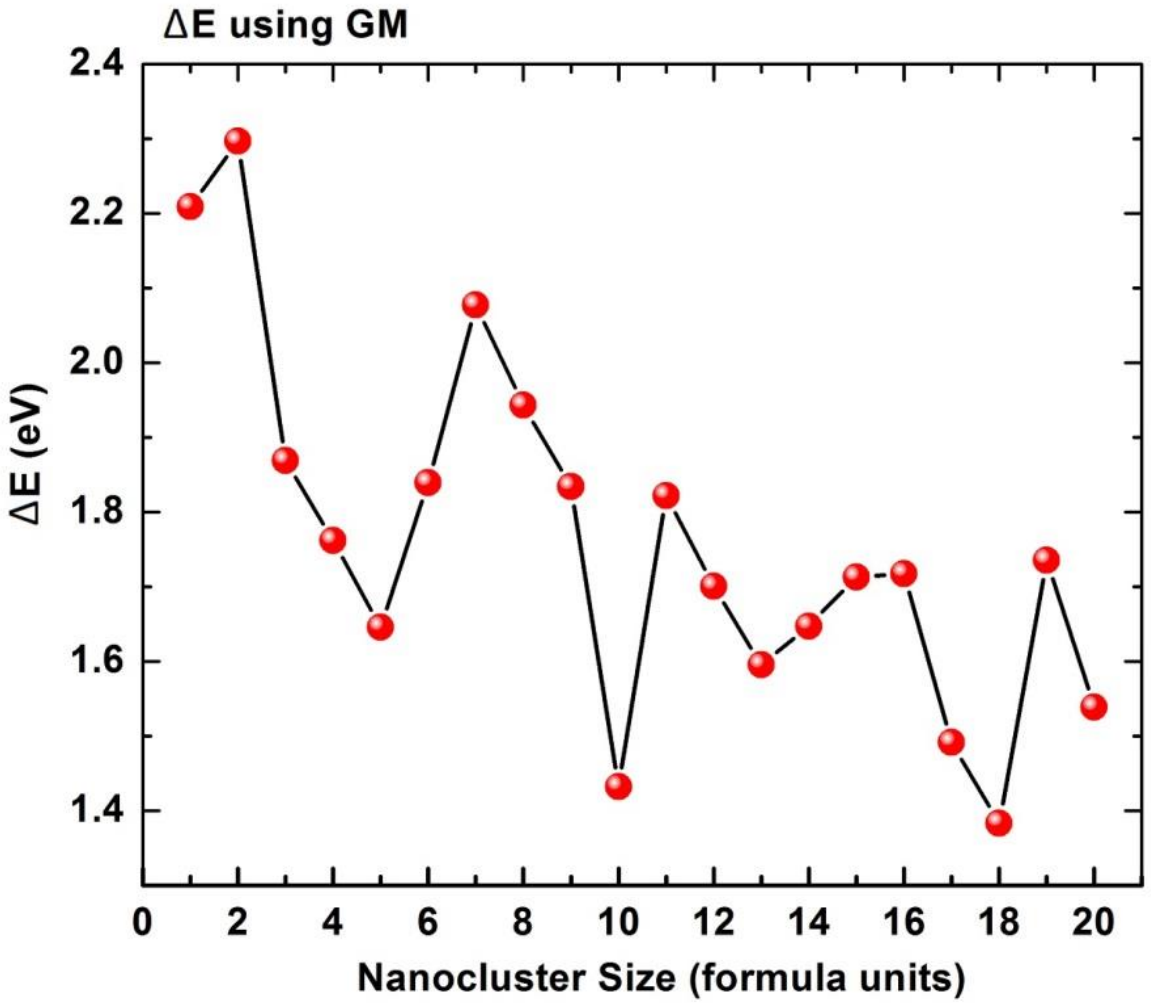

The energy difference between HOMO and LUMO, ΔE, for CeO_2 as a function of nanocluster size n (formula units).

(a)

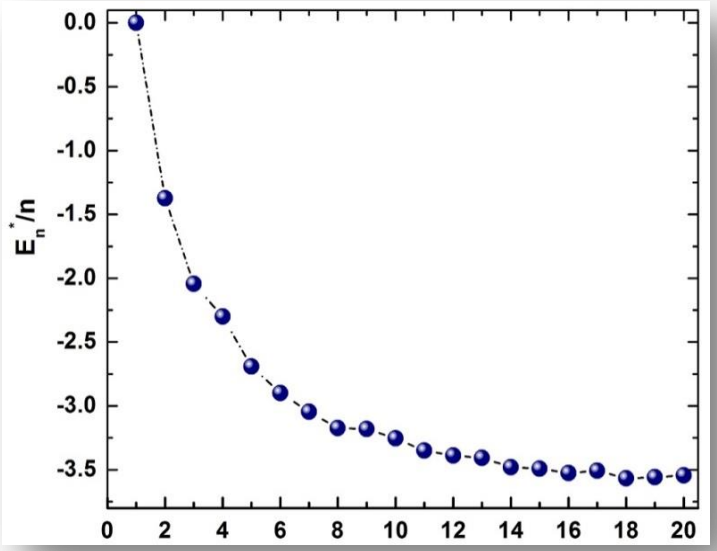

(b)

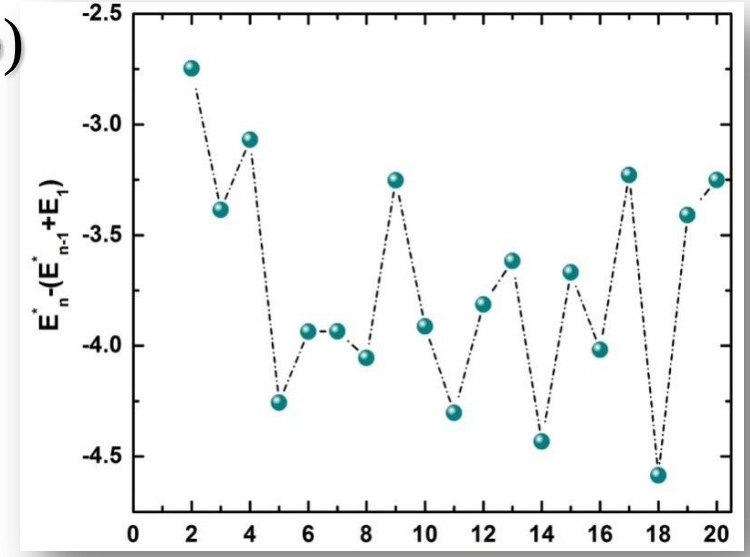

(c)

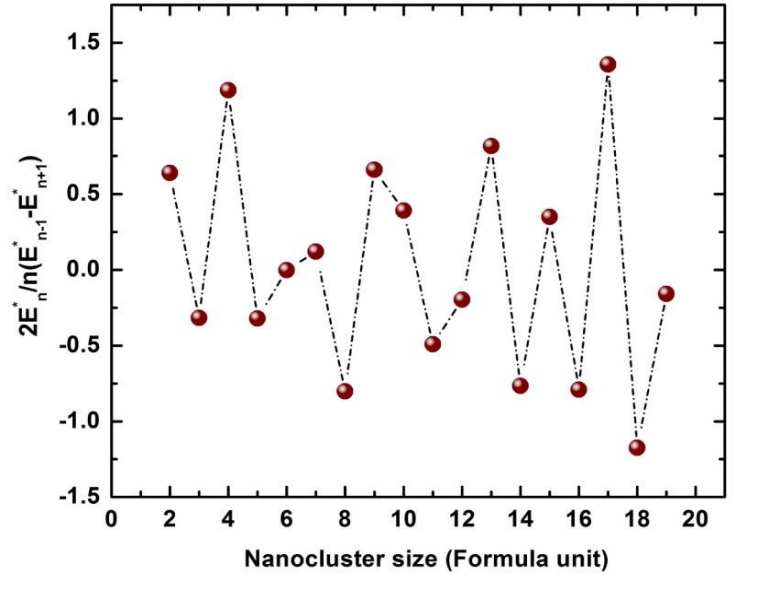

PBEsol energy (eV) for (a) binding energy per atom (b) fragmentation energy and (c) Second order difference of energy as a function of cluster size n (formula units)

Nickel Oxide Nanoclusters

Nickel oxide has a wide range of applications

- manufacturing of magnetic materials,
- alkaline battery cathodes,
- dye-sensitized solar cells,
- semiconductors,
- solid oxide fuel cells (SOFC),
- anti ferromagnetic layers,
- p-type transparent conducting films,
- electrochromic films,
- heterogeneous catalytic materials and
- gas sensors.
- nanocrystalline NiO powder shows superparamagnetism effect;
- drug delivery and MRI agent

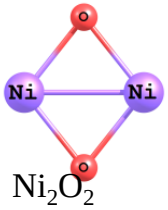

Ni_2O_2

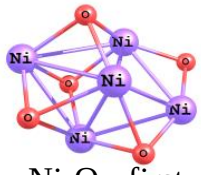

Ni_5O_5_first

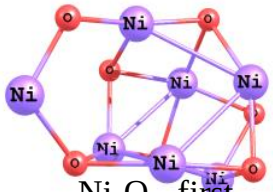

Ni_7O_7_first

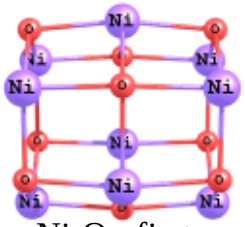

Ni_9O_9_first

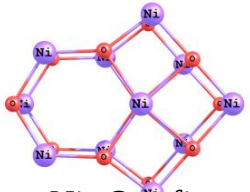

$Ni_{11}O_{11}$_first

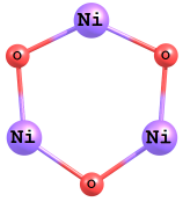

Ni_3O_3

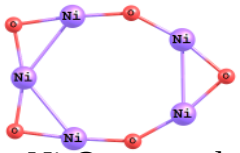

Ni_5O_5_second

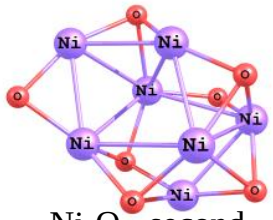

Ni_7O_7_second

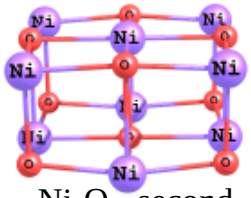

Ni_9O_9_second

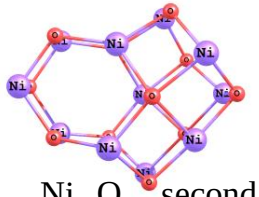

$Ni_{11}O_{11}$_second

Ni_4O_4_first

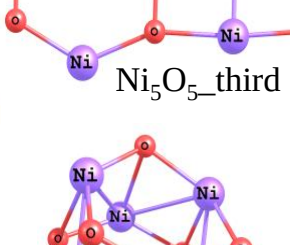

Ni_5O_5_third

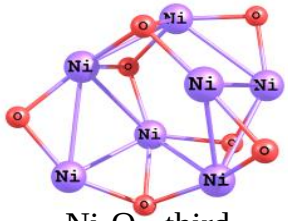

Ni_7O_7_third

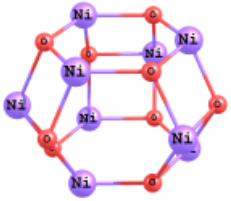

Ni_9O_9_third

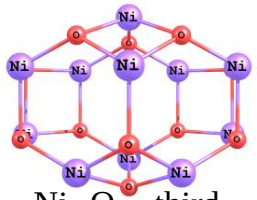

$Ni_{11}O_{11}$_third

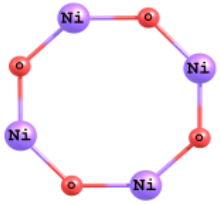

Ni_4O_4_second

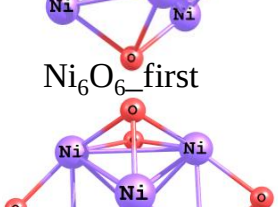

Ni_6O_6_first

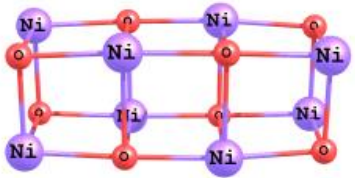

Ni_8O_8_first

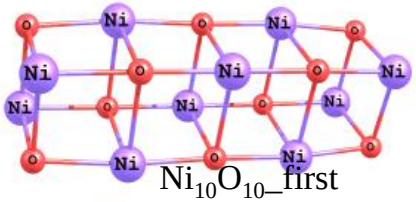

$Ni_{10}O_{10}$_first

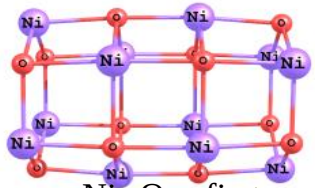

$Ni_{12}O_{12}$_first

Ni_6O_6_second

Ni_8O_8_second

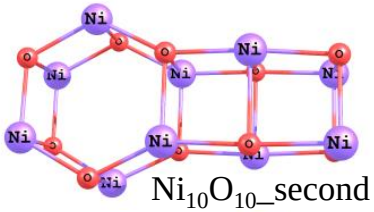

$Ni_{10}O_{10}$_second

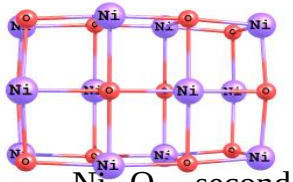

$Ni_{12}O_{12}$_second

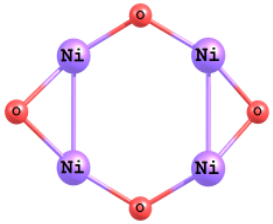

Ni_4O_4_third

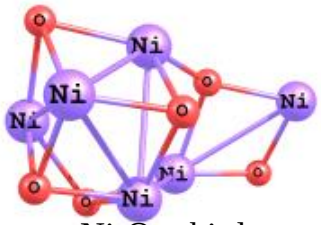

Ni_6O_6_third

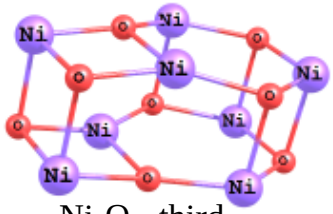

Ni_8O_8_third

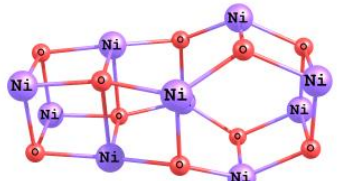

$Ni_{10}O_{10}$_third

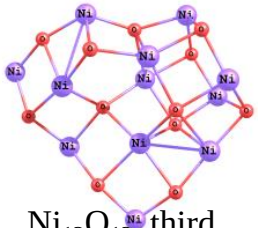

$Ni_{12}O_{12}$_third

$Ni_{13}O_{13}$_first

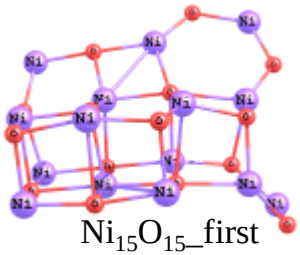

$Ni_{15}O_{15}$_first

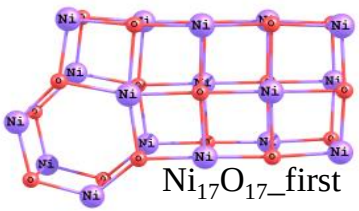

$Ni_{17}O_{17}$_first

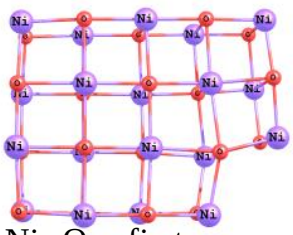

$Ni_{19}O_{19}$_first

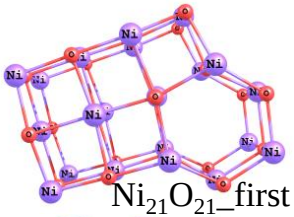

$Ni_{21}O_{21}$_first

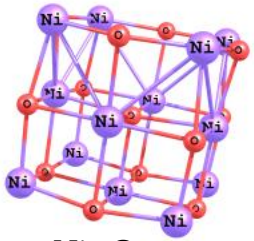

$Ni_{13}O_{13}$_second

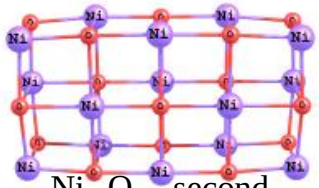

$Ni_{15}O_{15}$_second

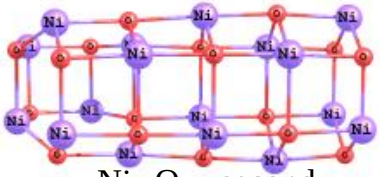

$Ni_{17}O_{17}$_second

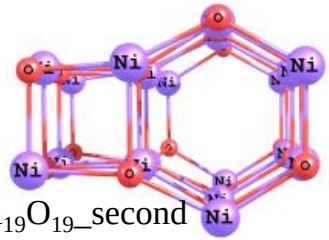

$Ni_{19}O_{19}$_second

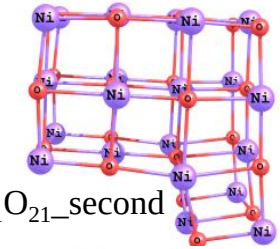

$Ni_{21}O_{21}$_second

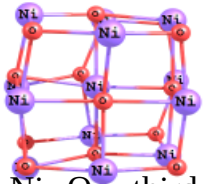

$Ni_{13}O_{13}$_third

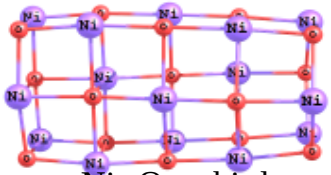

$Ni_{15}O_{15}$_third

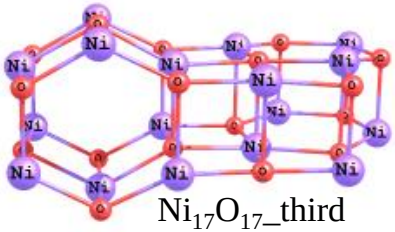

$Ni_{17}O_{17}$_third

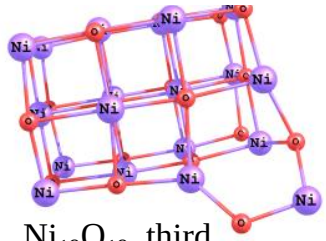

$Ni_{19}O_{19}$_third

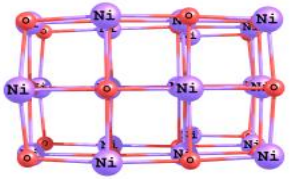

$Ni_{21}O_{21}$_third

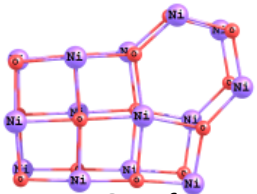

$Ni_{14}O_{14}$_first

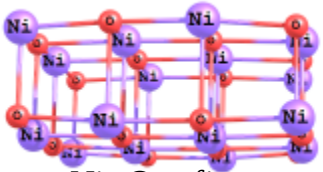

$Ni_{16}O_{16}$_first

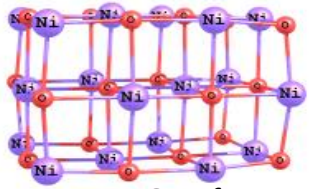

$Ni_{18}O_{18}$_first

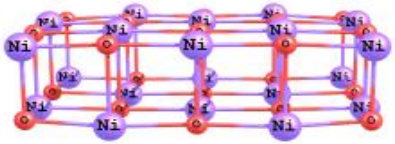

$Ni_{20}O_{20}$_first

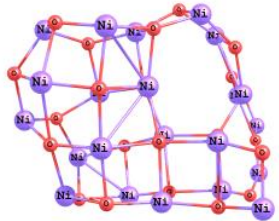

$Ni_{22}O_{22}$_first

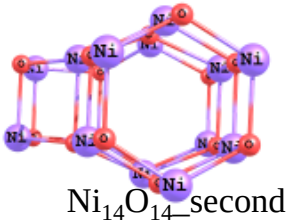

$Ni_{14}O_{14}$_second

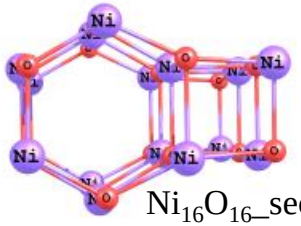

$Ni_{16}O_{16}$_second

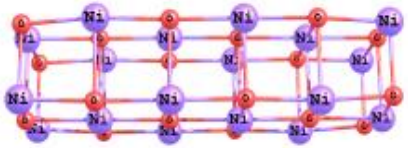

$Ni_{18}O_{18}$_second

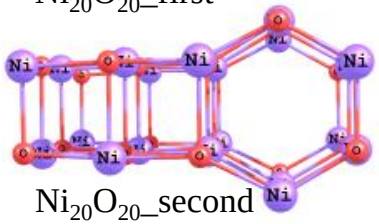

$Ni_{20}O_{20}$_second

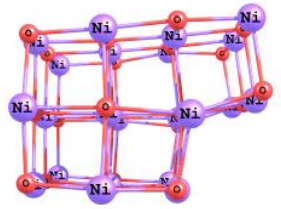

$Ni_{22}O_{22}$_second

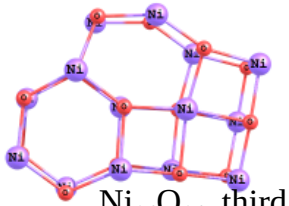

$Ni_{14}O_{14}$_third

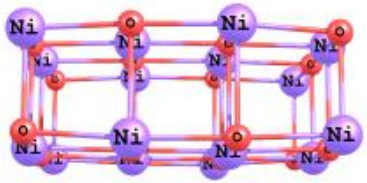

$Ni_{16}O_{16}$_third

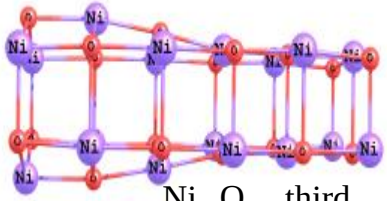

$Ni_{18}O_{18}$_third

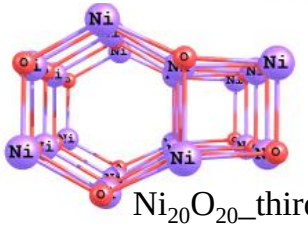

$Ni_{20}O_{20}$_third

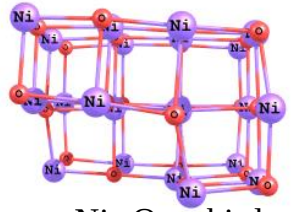

$Ni_{22}O_{22}$_third

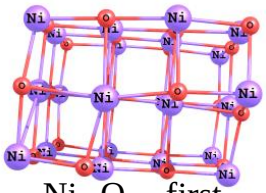
Ni$_{23}$O$_{23}$_first

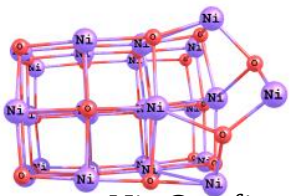
Ni$_{25}$O$_{25}$_first

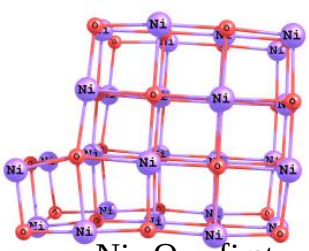
Ni$_{27}$O$_{27}$_first

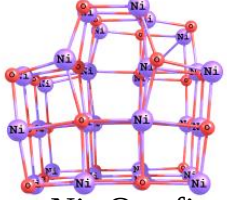
Ni$_{29}$O$_{29}$_first

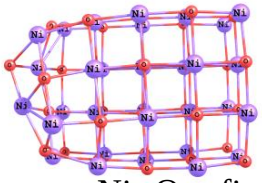
Ni$_{31}$O$_{31}$_first

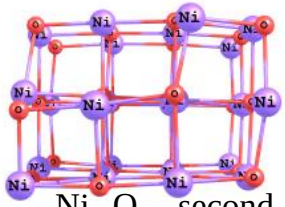
Ni$_{23}$O$_{23}$_second

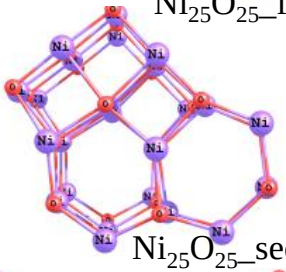
Ni$_{25}$O$_{25}$_second

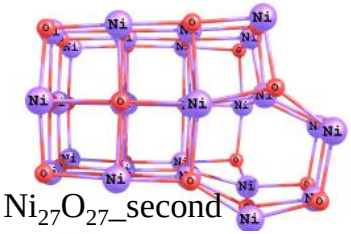
Ni$_{27}$O$_{27}$_second

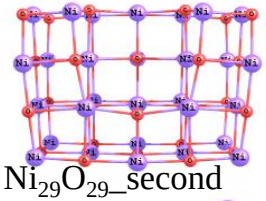
Ni$_{29}$O$_{29}$_second

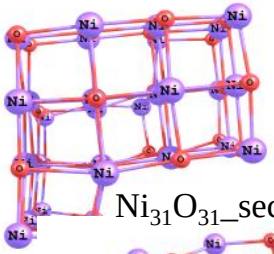
Ni$_{31}$O$_{31}$_second

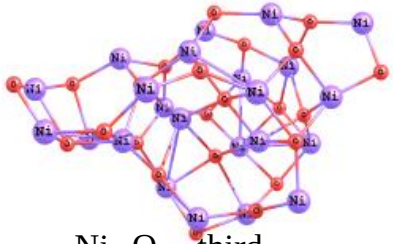
Ni$_{23}$O$_{23}$_third

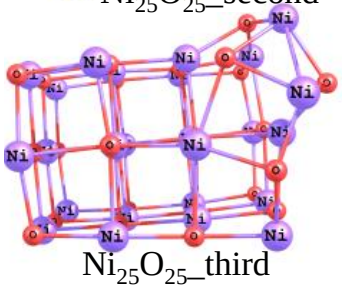
Ni$_{25}$O$_{25}$_third

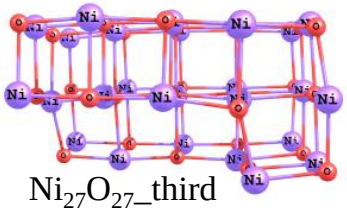
Ni$_{27}$O$_{27}$_third

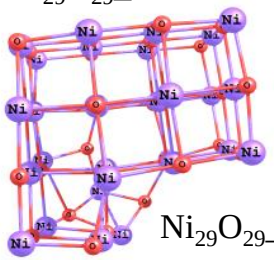
Ni$_{29}$O$_{29}$_third

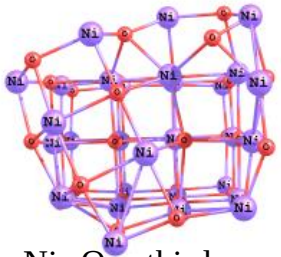
Ni$_{31}$O$_{31}$_third

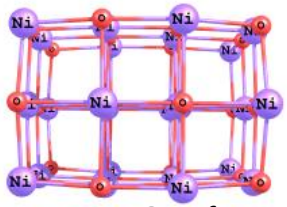
Ni$_{24}$O$_{24}$_first

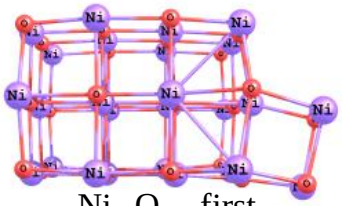
Ni$_{26}$O$_{26}$_first

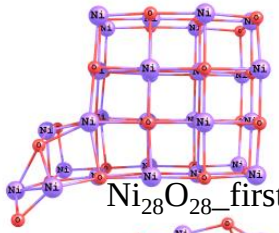
Ni$_{28}$O$_{28}$_first

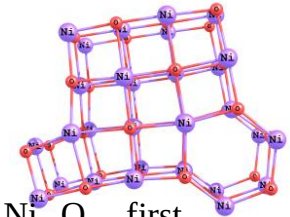
Ni$_{30}$O$_{30}$_first

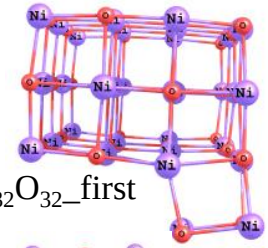
Ni$_{32}$O$_{32}$_first

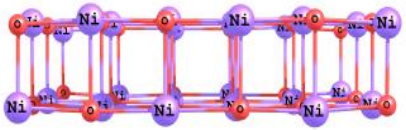
Ni$_{24}$O$_{24}$_second

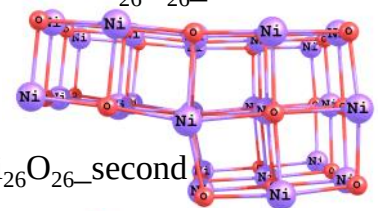
Ni$_{26}$O$_{26}$_second

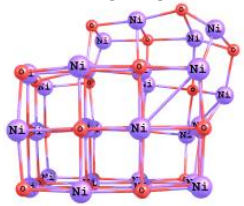
Ni$_{28}$O$_{28}$_second

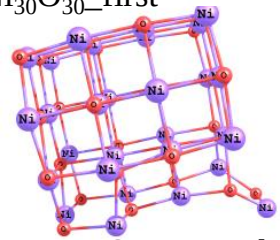
Ni$_{30}$O$_{30}$_second

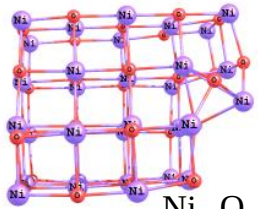
Ni$_{32}$O$_{32}$_second

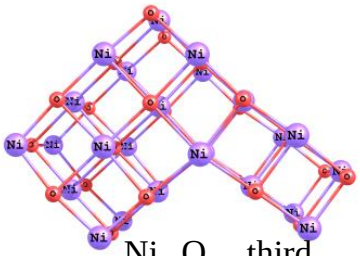
Ni$_{24}$O$_{24}$_third

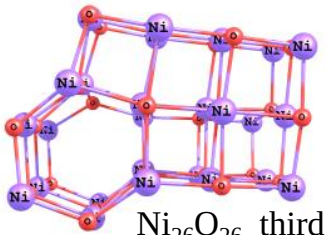
Ni$_{26}$O$_{26}$_third

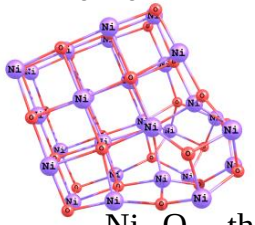
Ni$_{28}$O$_{28}$_third

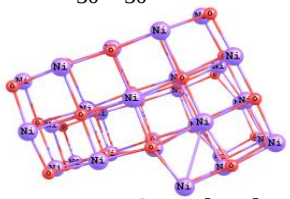
Ni$_{30}$O$_{30}$_third

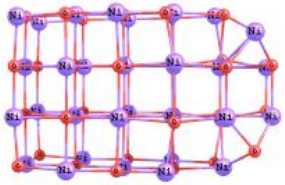
Ni$_{32}$O$_{32}$_third

DFT Studies on nickel oxide nanoclusters

- A series of nickel oxide nanoclusters, Ni_nO_n (n=2 to 7) is studied and tried to correlate their possible structures with their magnetic properties.

- Zero-field splitting (ZFS) parameter D-tensor and g-tensors are being calculated for this series of NiO clusters.

- EPR studies of transition metal systems were successfully done earlier wherein it is showed that the theoretical magnetic parameters give fruitful values when compared to the experimental results.

EPR parameters: g-Tensor and D-tensor

- Electronic g-tensors provide insight in electronic interactions on the unpaired electrons of a system.
- The decomposed form of electronic g-tensor is:

$$g = g_e 1 + \Delta g$$

where 'g'=electronic g-tensor, g_e=g-factor for free electron (2.0023) and Δg=g-tensor shift.

- The D-tensor (or ZFS parameter) describes the removal of the state degeneracy for systems with S > 1/2 in absence of magnetic field.

$$H_{ZFS} = D\left[S_z^2 - \frac{1}{3}S(S+1)\right] + E\left(S_x^2 - S_y^2\right)$$

- D-tensor is known to be constituted by two parameters:
  - Spin-orbit coupling (SOC) and
  - Spin-spin coupling (SSC).
- Single-molecule magnets (SMMs) have negative sign for D-tensor.

- KLMC generated geometries are re-optimized and their energies are calculated in the FHI-aims software.
- Single point calculation of the magnetic properties are done in ORCA program Package.
- Basis sets used:
  - For the Ni atoms Stuttgart/Dresden ECPs (SDD) and def2-TZVP Ahlrichs basis set for Coulomb fitting is used.
  - For the O atom def2-TZVP basis set is used.
- Functional used:
  - B3LYP functional.

- For spin-orbit coupling (SOC) contribution:
  - For transition metals, for which the relativistic effects are significant, the spin-orbit coupling (SOC) for D-tensors and the g-tensors are calculated using the spin-orbit mean-field (SOMF) operator.
  - The Coupled Perturbed (CP) method is employed that solves a set of coupled-perturbed equations for the SOC perturbation.

- For spin-spin coupling (SSC) contribution:
  - This is an expectation value which involves spin-density of the system.
  - Canonical orbitals are being used.

Optimized geometries from FHI-aims

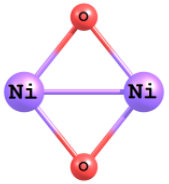

Ni_2O_2

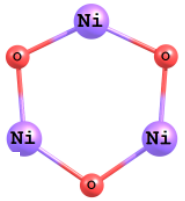

Ni_3O_3

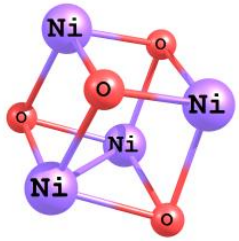

Ni_4O_4_first

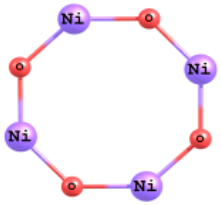

Ni_4O_4_second

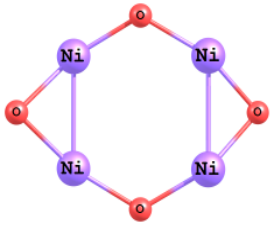

Ni_4O_4_third

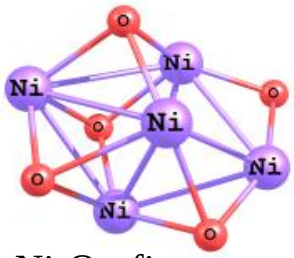

Ni_5O_5_first

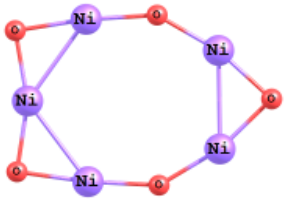

Ni_5O_5_second

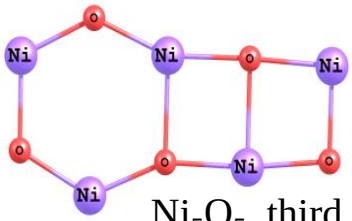

Ni_5O_5_third

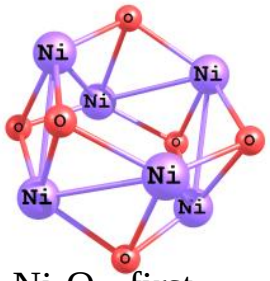

Ni_6O_6_first

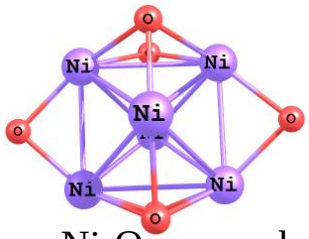

Ni_6O_6_second

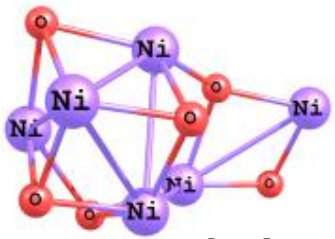

Ni_6O_6_third

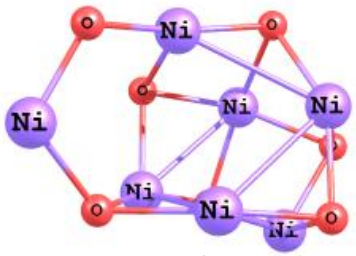

Ni_7O_7_first

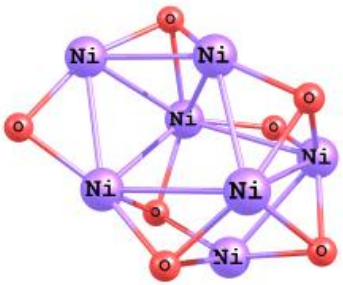

Ni_7O_7_second

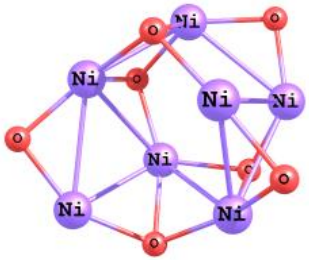

Ni_7O_7_third

EPR parameters from ORCA

Cluster	Energies (in Hartree)	D-tensor (in cm^{-1})	g-Tensor			g_{iso}
			g_x	g_y	g_z	
Ni_2O_2	**-3205.37**	**59.063**	1.786	1.815	2.031949	**1.878**
Ni_3O_3	**-4808.14**	**50.893**	1.968	2.180	2.184159	**2.111**
Ni_4O_4_first	**-6410.92**	**28.804**	1.994	2.077	2.155938	**2.076**
Ni_4O_4_second	**-6410.89**	**84.527**	1.730	2.126	2.453003	**2.103**
Ni_4O_4_third	**-6410.92**	**109.181**	1.955	2.124	2.245205	**2.108**
Ni_5O_5_first	**-8013.61**	**-39.801**	1.976	2.161	2.209788	**2.116**
Ni_5O_5_second	**-8013.69**	**-43.310**	1.796	2.150	2.295258	**2.080**
Ni_5O_5_third	**-8013.69**	**53.952**	1.848	2.195	2.285124	**2.109**
Ni_6O_6_first	**-9616.35**	**16.309**	2.032	2.116	2.147406	**2.098**
Ni_6O_6_second	**-9616.41**	**105.268**	2.004	2.047	2.304309	**2.118**
Ni_6O_6_third	**-9616.42**					
Ni_7O_7_first	**-11211.0495**					
Ni_7O_7_second	**-11219.17944**					
Ni_7O_7_third	**-11219.18231**					

- Depending on the sign, the magnetization is aligned along an easy axis (negative D) or within an easy plane (positive D).
- Most of the clusters have positive D-tensors and this implies they are not suitable to be used as single-molecule magnets.
- Little difference in orbital reduction factor or the respective covalencies between Ni and O atom result in positive D-values.
- Positive D-tensor corresponds to non-magnetic $M_S=0$ state at ground state, while for negative D-value $M_S=0$ is highest in energy at zero-field.

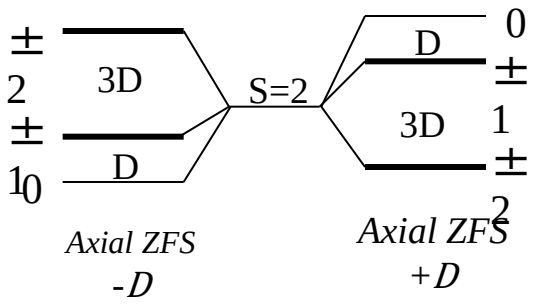

- The g-tensor values show significant deviations from free electron g-value (2.0023).
  - This confirms anisotropic behavior of the NiO clusters in presence of external magnetic field.
- According to Mulliken gross atomic population, approximately 70% of charge is localized on the Ni atoms and hence larger contribution to g-tensor comes from the spin-orbit coupled with orbital Zeeman effect.
  - Enhanced contribution from the metal orbitals give rise to *g* anisotropy.
- Highest contribution for total g-tensor comes from the relativistic mass-correction term (Δg_{RMC}) which is true for most of the systems involving transition metal.

- Size dependent properties of metal nanoclusters using DFT
- Structural and electronic properties of metal clusters,
- Metal clusters in catalysis:
  - CO oxidation,
  - Reverse hydrogen spillover,
  - NO oxidation,
  - Methane oxidation
- Metal oxide nanoclusters
- Catalysis by oxide nanocluster

The lowest-energy structures of gold cluster, Au_n with n=2-13

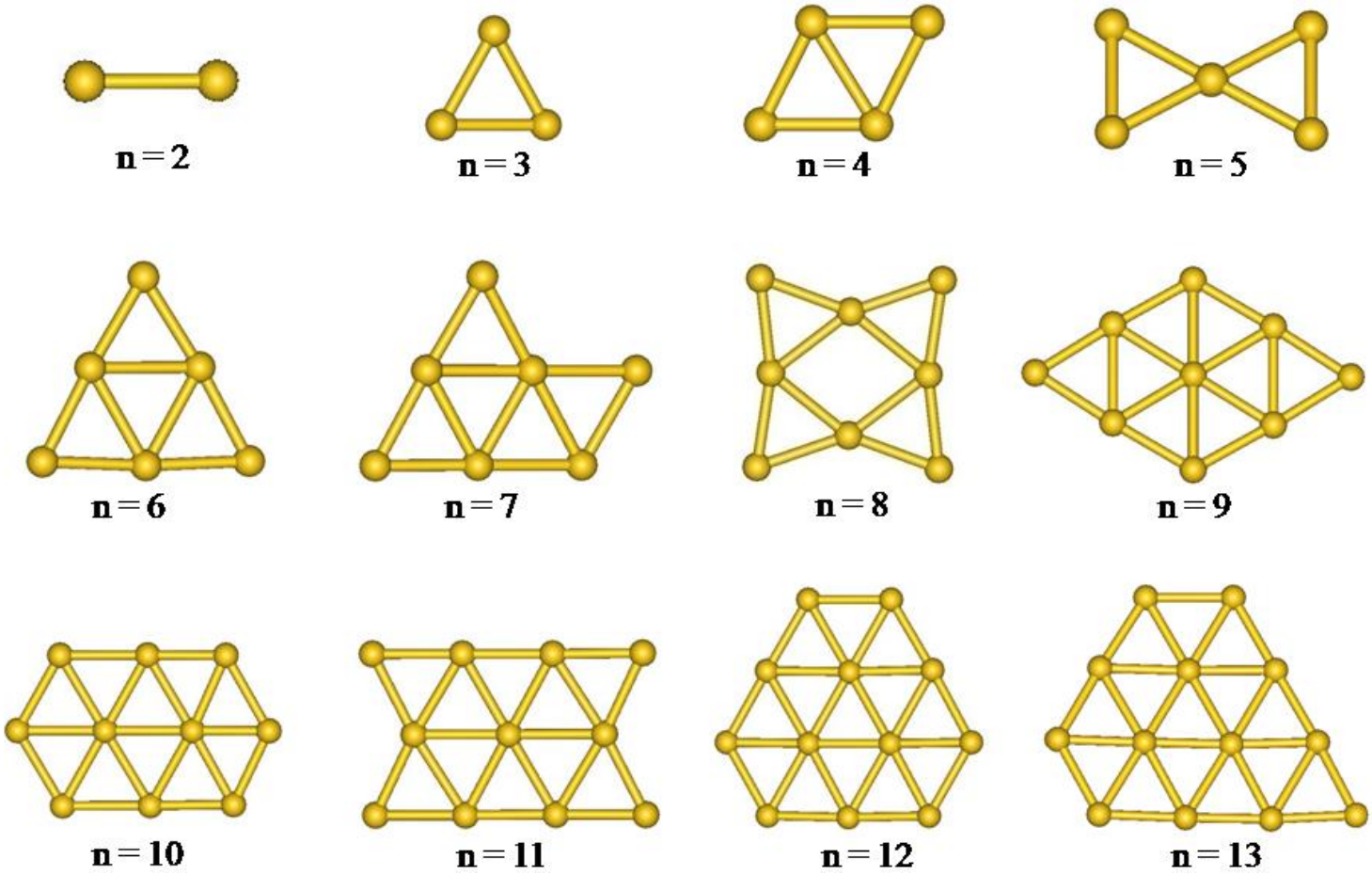

Planar to 3D transition: at n=7, Hakkinen & Landman, GGA, Phys. Rev. B, 62, R2287, 2000

at n=11, Walker, LDA, JCP, 122, 94310, 2005

at n =15, Wang et al, DFT (PW91), CPL, 392, 452, 2004.

Deka & Deka Theochem, 870 (2008) 83-93

Average bond length, binding energy per atom and fragmentation energy

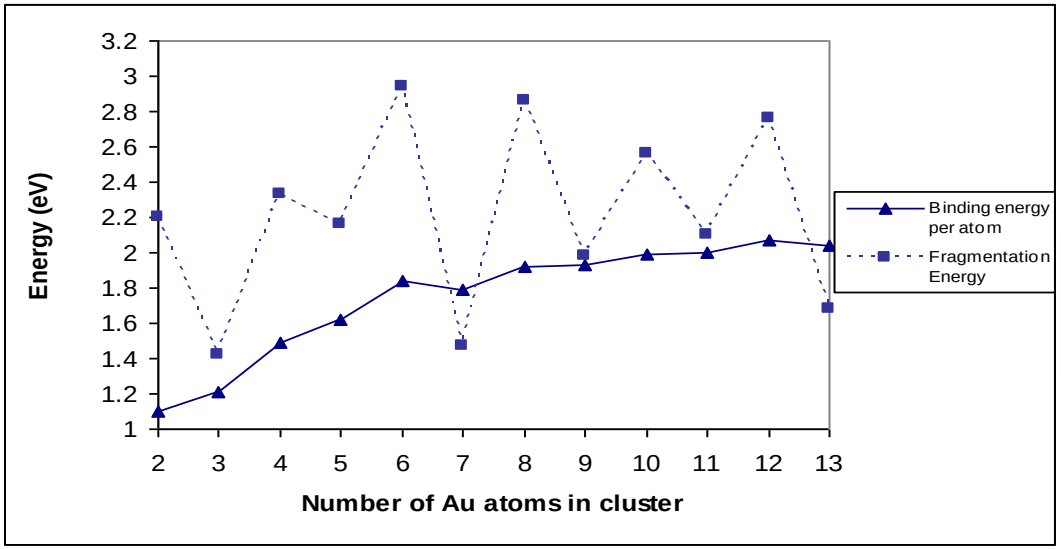

$E_b = nE(Au_1) - E(Au_n)$

Binding energy per atom = E_b/n

The fragmentation energy:

$D(n,n-1) = E_{n-1} + E_1 - E_n$

- ✓ **Odd-even oscillation**
- ✓ **Even numbered clusters are more stable**

n	Eb/n(eV)	D(eV)	Ave Coor. No.
1			
2	1.102	2.203	1.00
3	1.209	1.423	1.33
4	1.490	2.334	2.50
5	1.623	2.156	2.80
6	1.843	2.940	3.00
7	1.790	1.474	3.43
8	1.923	2.856	3.00
9	1.930	1.982	3.56
10	1.993	2.560	3.80
11	2.002	2.097	3.82
12	2.066	2.765	4.00
13	2.036	1.676	4.00

CO oxidation

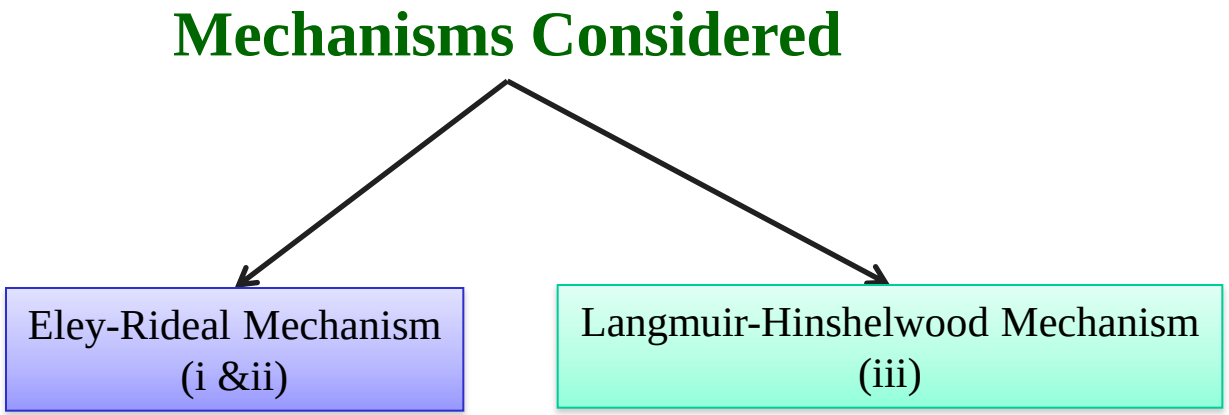

(i) $CO(g) + O_2(ads)$

(ii) $CO(ads) + O_2(g)$ → $CO_2(g)$

(iii) $CO(ads) + O_2(ads, diss)$

Gas phase neutral, cationic and anionic palladium (Pd_n, n=2–13) clusters

Computational details for all gas phase calculations:

DMol^3 program

DNP basis set

BLYP functional

$$BE = -E_{tot}^{0,\pm} / n$$

$$E_{tot}^{0} = E_n - nE_1$$

$$E_{tot}^{\pm} = E_n^{\pm} - (n-1)E_1 - E_1^{\pm}$$

$$S(n) = E_{n+1}^{tot} + E_{n-1}^{tot} - 2E_n^{tot}$$

$$S^{\pm}(n) = E_{n+1}^{\pm(tot)} + E_{n-1}^{\pm(tot)} - 2E_n^{\pm(tot)}$$

$$E_{n\rightarrow(n-1)+1} = E_{n-1} + E_1 - E_n, n \geq 1$$

$$IP = E_n^{+} - E_n$$

$$EA = E_n - E_n^{-}$$

$$\eta = \frac{IP - EA}{2}$$

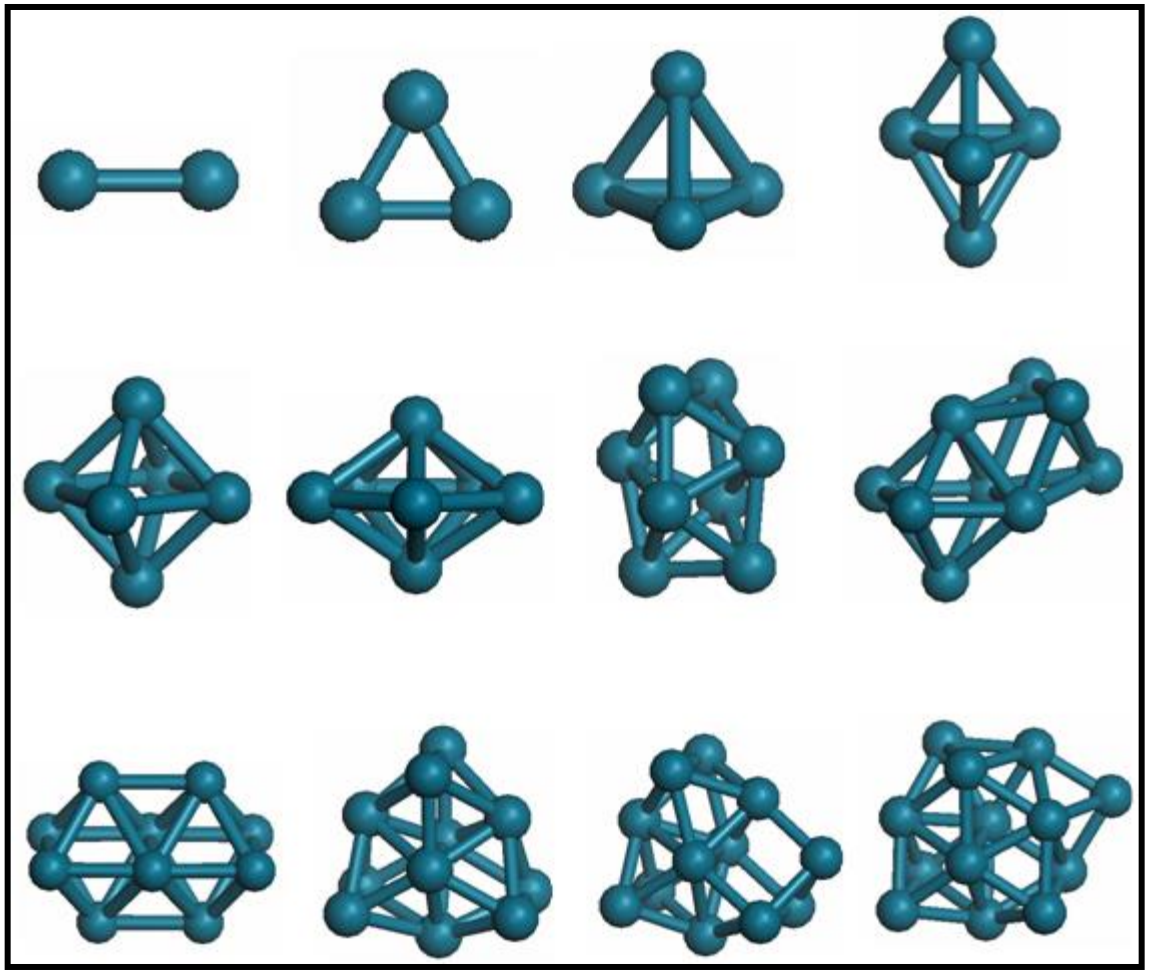

Lowest energy structures of neutral, cationic and anionic Pd_n (n=2–13) clusters

Kalita & Deka J. Chem. Phys. 127, 2007, 244306

The reaction proceeds via following steps:

$Pd_4+O_2 \rightarrow Pd_4–O2$ (-0.82, -0.38, -1.51 eV)

$Pd_4+O_2+CO \rightarrow Pd_4–O_2–CO$ (-2.27, -1.72, -3.33 eV)

$Pd_4+O_2+CO \rightarrow Pd_4–O–CO_2$ (-3.96, -4.03, -4.81 eV)

$Pd_4+O_2+CO \rightarrow Pd_4–O+CO_2$ (-3.56, -3.57, -4.08 eV)

$$Pd_4+O_2+CO \rightarrow Pd_4O+CO_2$$

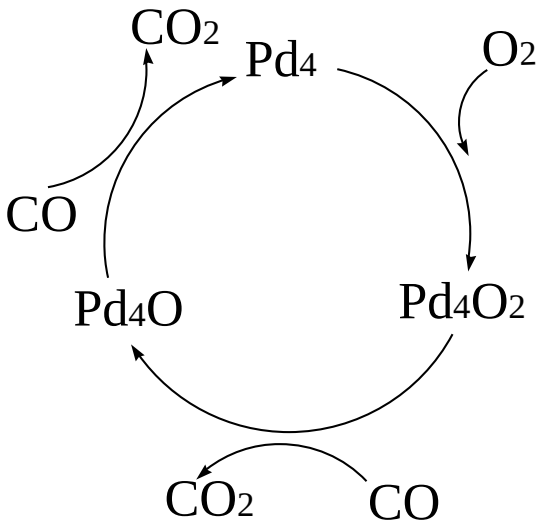

Catalytic cycle of CO oxidation on neutral, cationic and anionic Pd_4 clusters: atomic oxygen reacting with CO

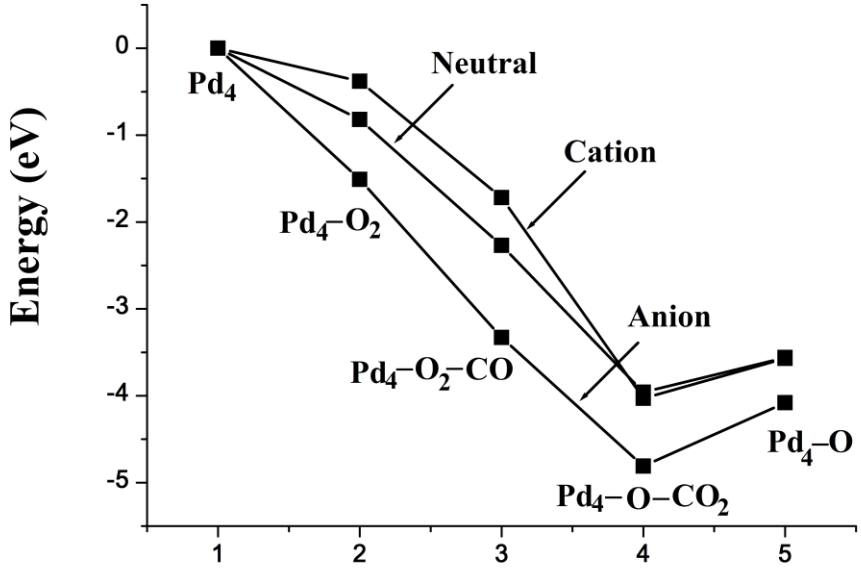

The energetic profile of complete reaction cycle for CO oxidation on neutral, cationic and anionic Pd_4 clusters: molecular oxygen reacting with CO

Kalita & Deka, J. Am. Chem. Soc. 131 (2009) 13252-13254

The reaction proceeds via following steps:

$Pd_4+O_2 \rightarrow Pd_4–O_2$ (-0.82, -0.38, -1.51 eV)

$Pd_4+O_2 \rightarrow Pd_4–2O$ (-1.63, -1.21, -2.63 eV)

$Pd_4+O_2+CO \rightarrow Pd_4–2O–CO$ (-3.28, -2.68, -4.77 eV)

$Pd_4+O_2+CO \rightarrow Pd_4–O–CO_2$ (-3.96, -4.03, -4.81 eV)

$Pd_4+O_2+CO \rightarrow Pd_4–O+CO_2$ (-3.56, -3.57, -4.08 eV)

$$Pd_4+2O+CO \rightarrow Pd_4O+CO_2$$

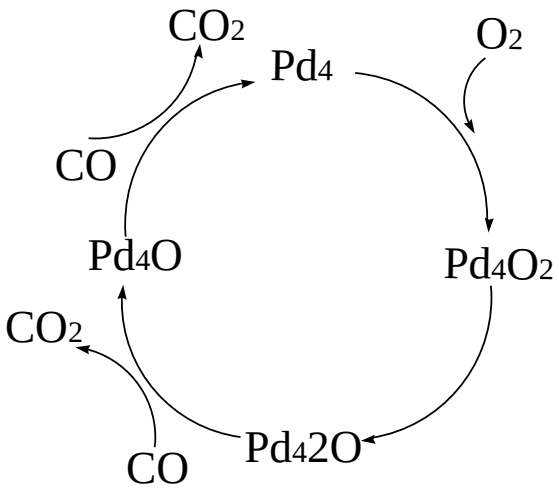

Catalytic cycle of CO oxidation on neutral, cationic and anionic Pd_4 clusters: atomic oxygen reacting with CO

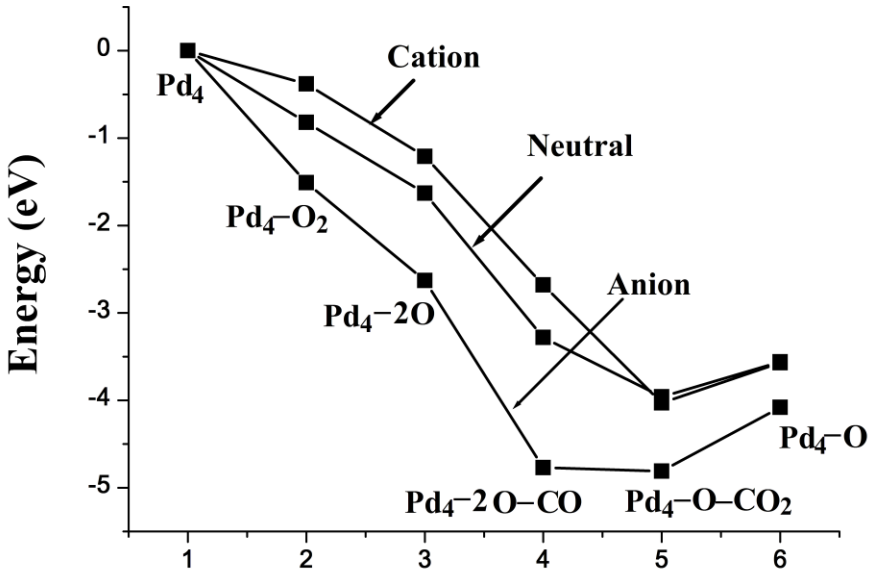

The energetic profile of complete reaction cycle for CO oxidation on neutral, cationic and anionic Pd_4 clusters: dissociated oxygen reacting with CO

Kalita & Deka, J. Am. Chem. Soc. 131 (2009) 13252-13254

The reaction proceeds via following steps:

$Pd_4 + \frac{1}{2} O_2 \rightarrow Pd_4–O$ (-0.66, -0.67, -1.19 eV)

$Pd_4 + \frac{1}{2} O_2 + CO \rightarrow Pd_4–O–CO$ (-2.25, -2.25, -3.12 eV)

$Pd_4 + \frac{1}{2} O_2 + CO \rightarrow Pd_4–CO_2$ (-2.81, -3.07, -3.88 eV)

$Pd_4 + \frac{1}{2} O_2 + CO \rightarrow Pd_4 + CO_2$ (-2.89, -2.89, -2.89 eV)

$$Pd_4 + O + CO \rightarrow Pd_4 + CO_2$$

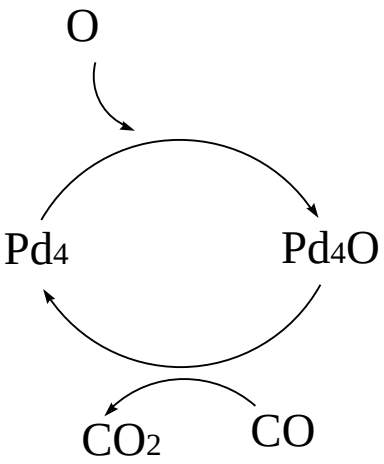

Catalytic cycle of CO oxidation on neutral, cationic and anionic Pd_4 clusters: atomic oxygen reacting with CO

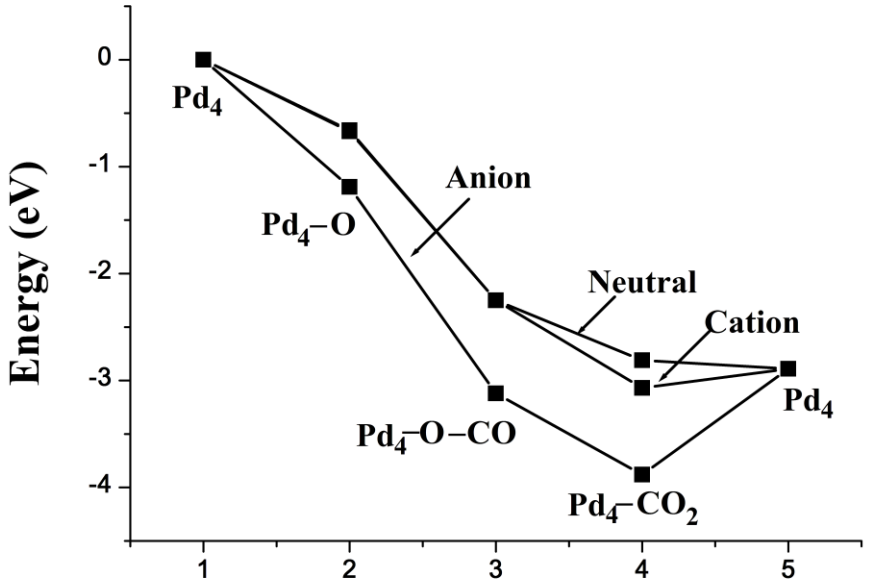

The energetic profile of complete reaction cycle for CO oxidation on neutral, cationic and anionic Pd_4 clusters: atomic oxygen reacting with CO

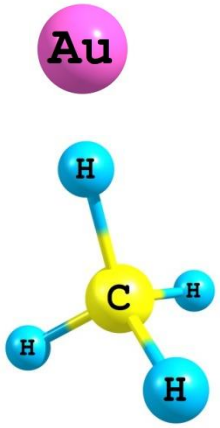

CH_4

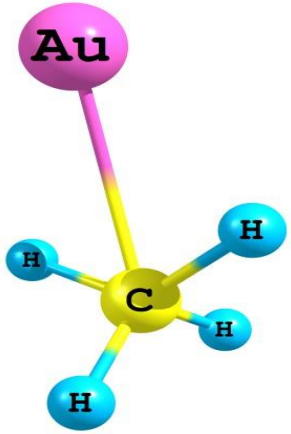

Au^+CH_4

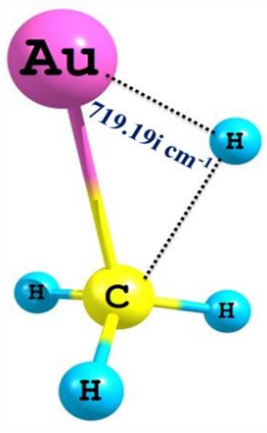

TS1

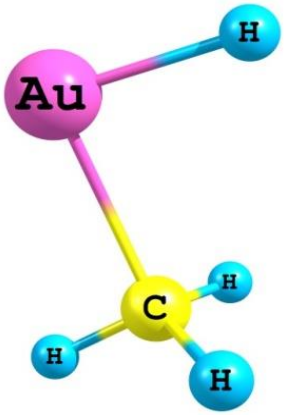

IM1

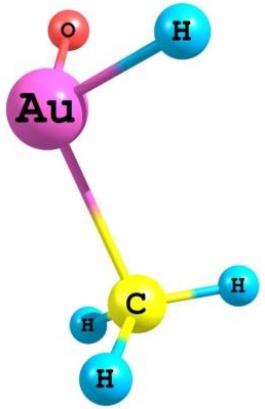

IM2

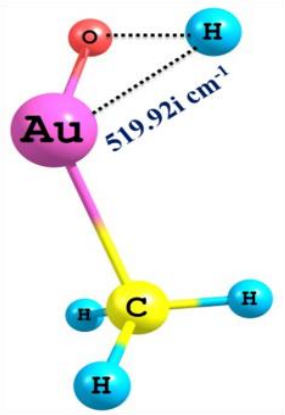

TS2

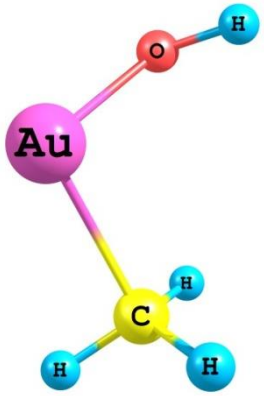

IM3

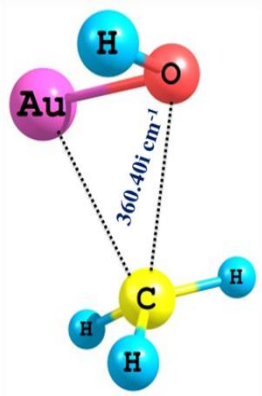

TS3

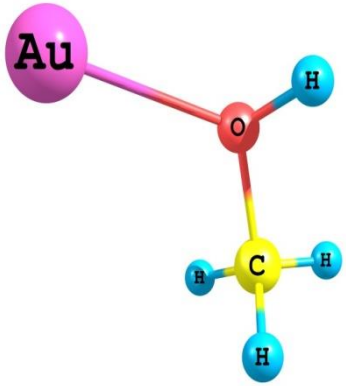

IM4

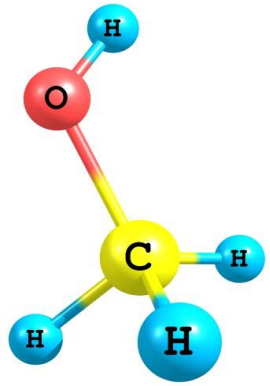

CH_3OH

Optimized geometries of reactants, intermediates(IM), transition states(TS) & products

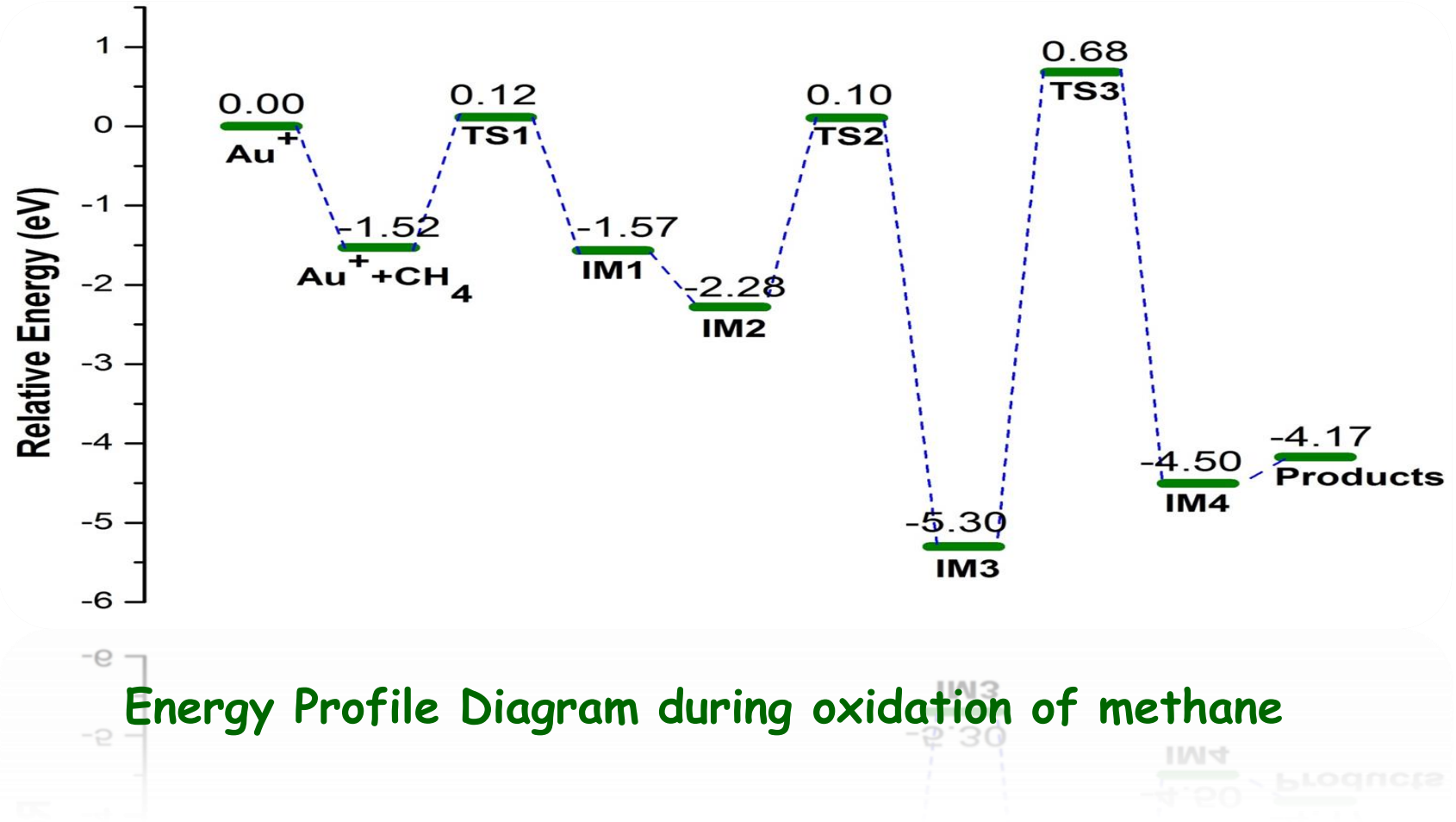

Energy Profile Diagram during oxidation of methane

✓The step involving TS3 i.e., the formation of CH_3OH is the most energetic step and rate determining step of the reaction.

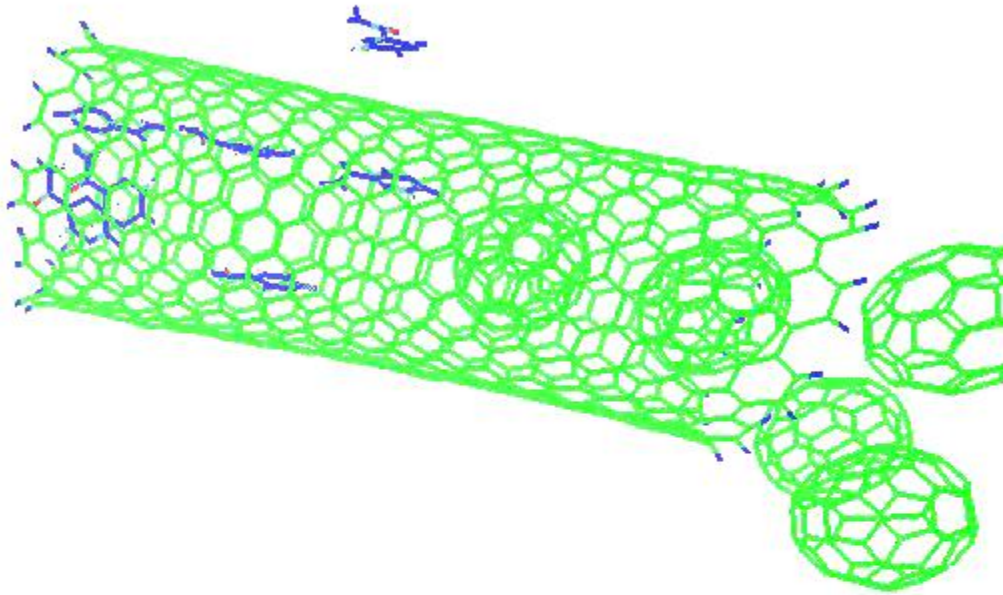

N. Saikia and R. C. Deka, J. Phys. Chem. Lett. 4 (2013) 4126-4132

Prof. Kimihiko Hirao, Prof. C. R. A. Catlow, FRS, S. M. Woodley of UCL

DST, JSPS

Thank You